Insights into searches for the nanohertz gravitational-wave background with a Fisher analysis

Yacine Ali-Haïmoud (NYU)

based on arXiv:2006.14570, 2010.13958

with Tristan Smith and Chiara Mingarelli

King's College London seminar, May 19, 2021

Painting by H.J. Detouche

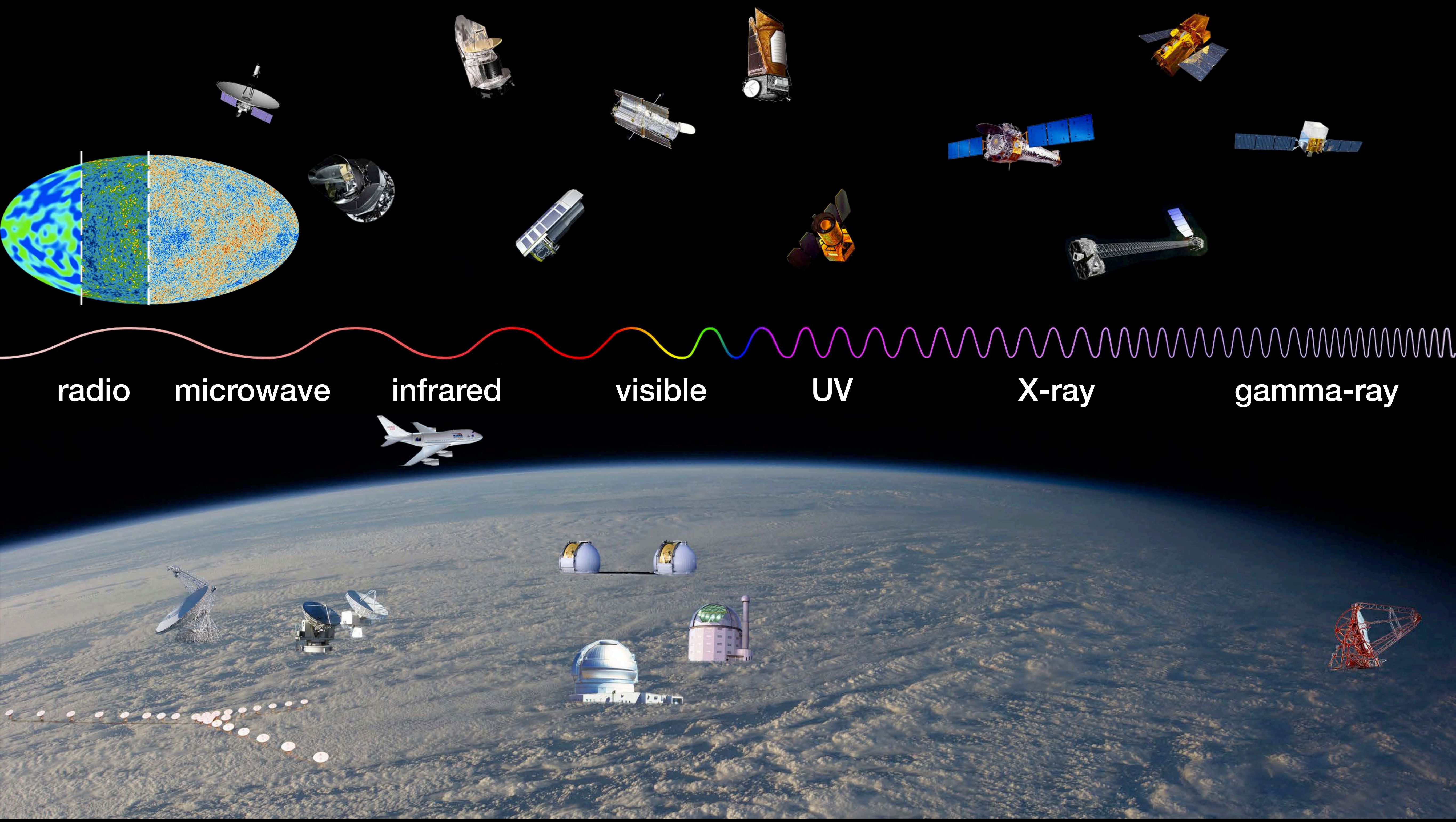
radio
microwave
infrared
visible
UV
X-ray
gamma-ray

The CMB success story

1965: Penzias & Wilson detect "excess emission" of **3 K**, interpreted as the CMB by **Dicke, Peebles, Roll & Wilkinson**

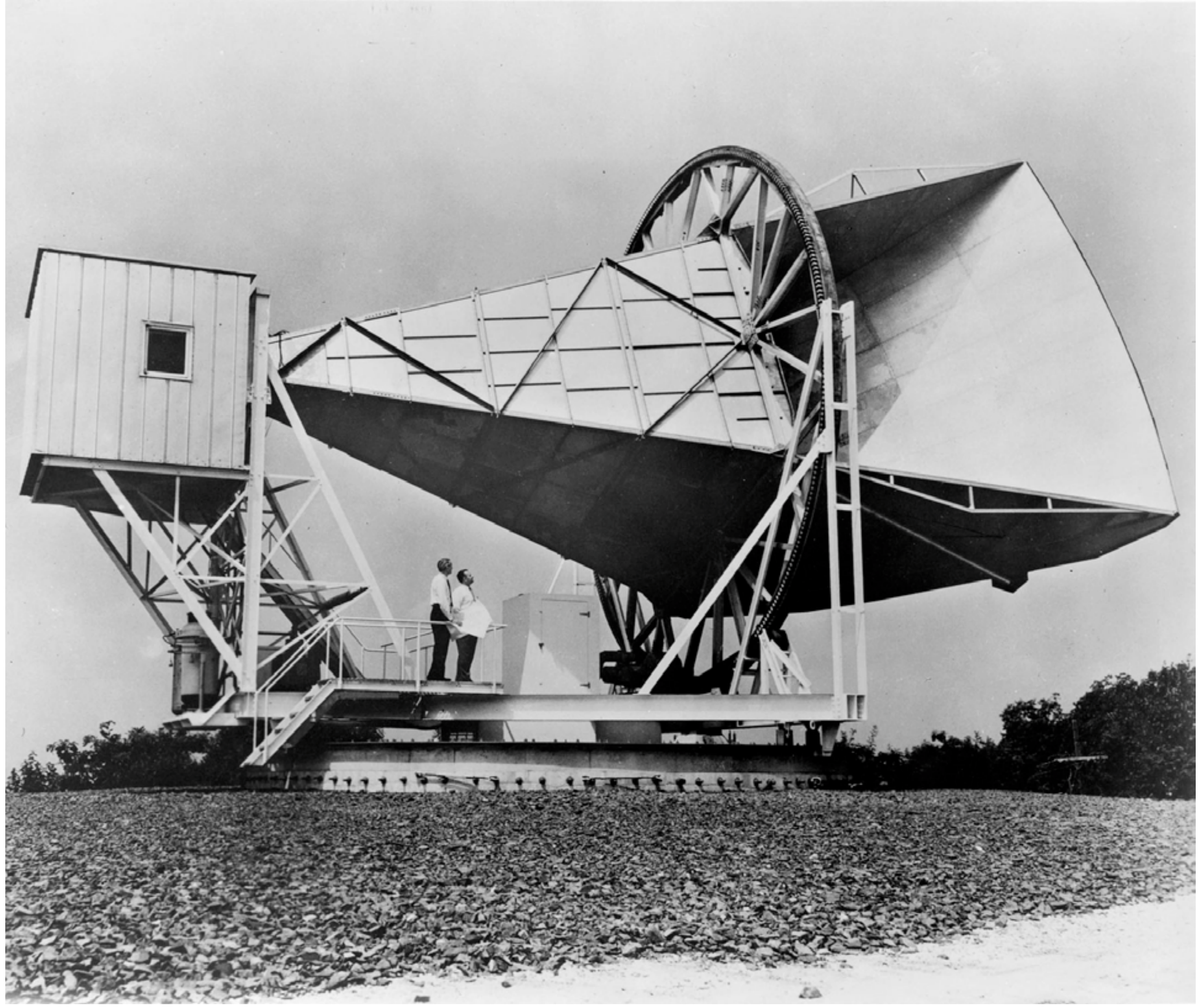

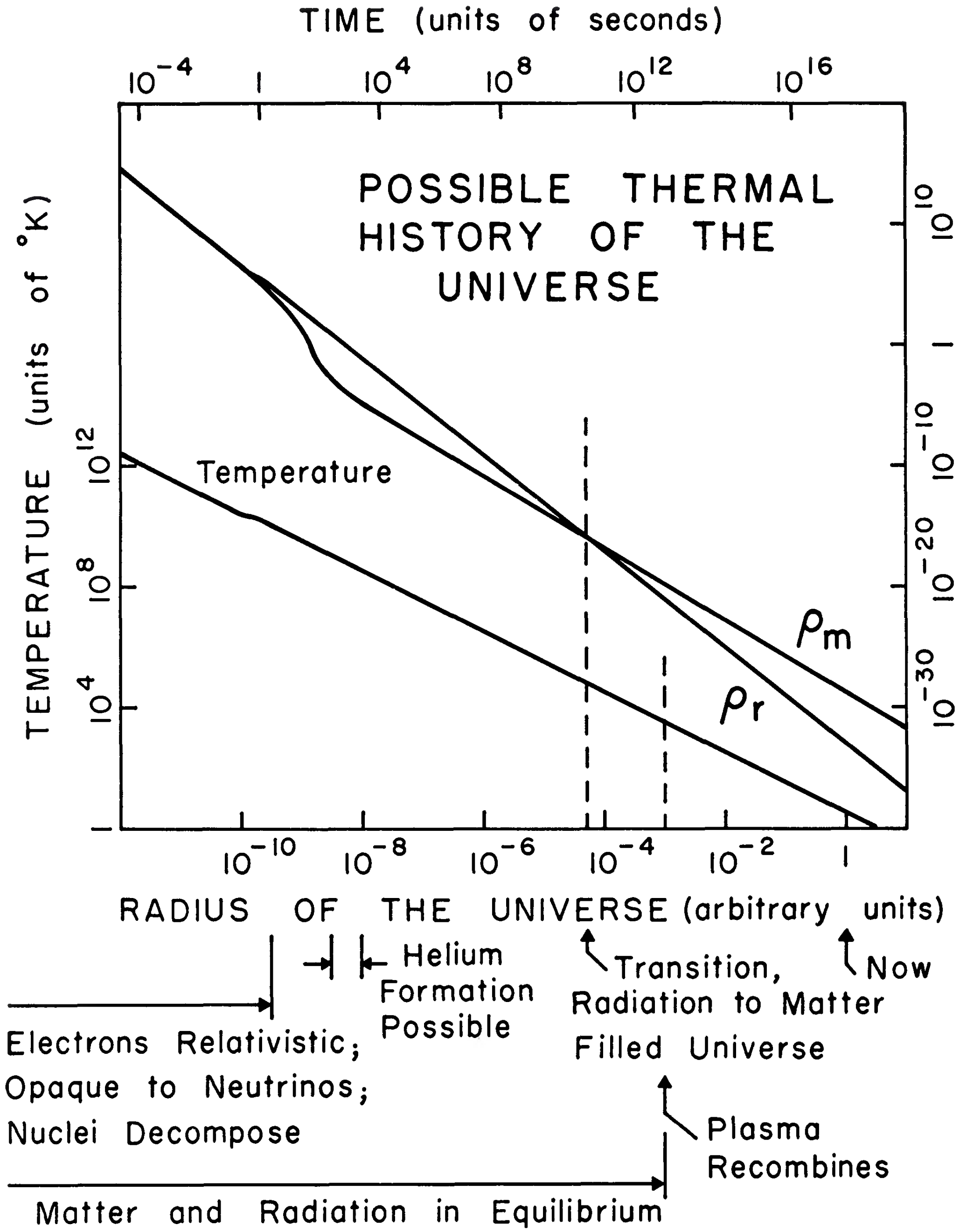

The CMB success story

1990: the CMB has a perfect blackbody spectrum with distortions < 1% (improved to < 0.01%, Mather et al. 1999)

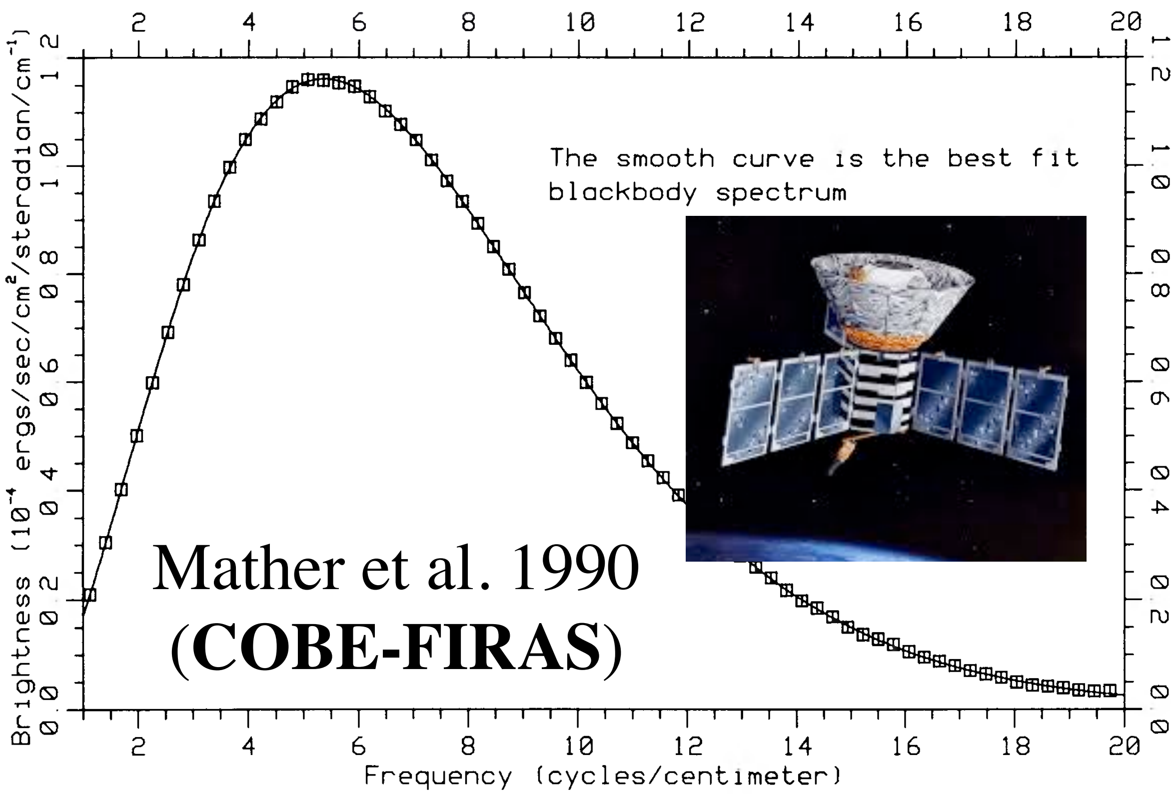

FIG. 2.—Preliminary spectrum of the cosmic microwave background from the FIRAS instrument at the north Galactic pole, compared to a blackbody.

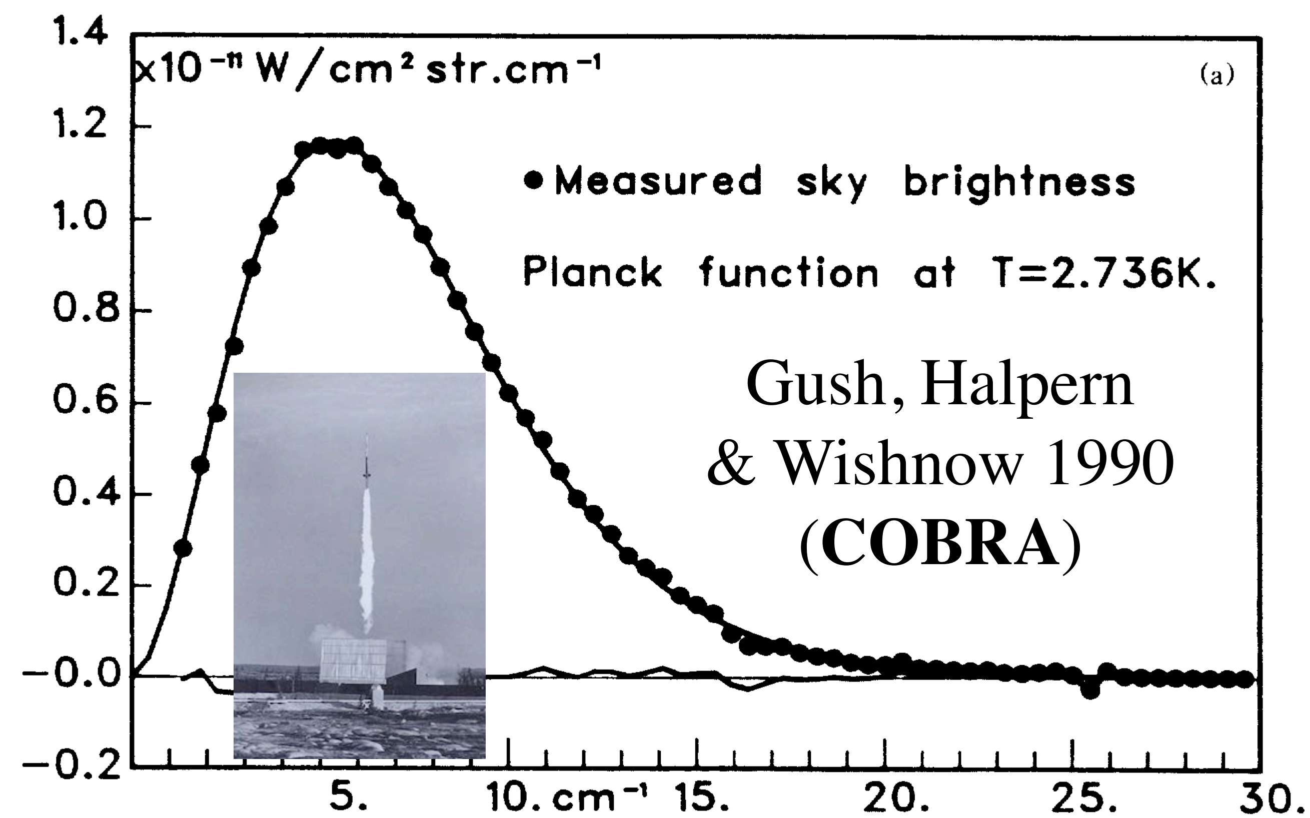

=> Stringent bounds on energy injection/extraction since a few months after the Big Bang

The CMB success story

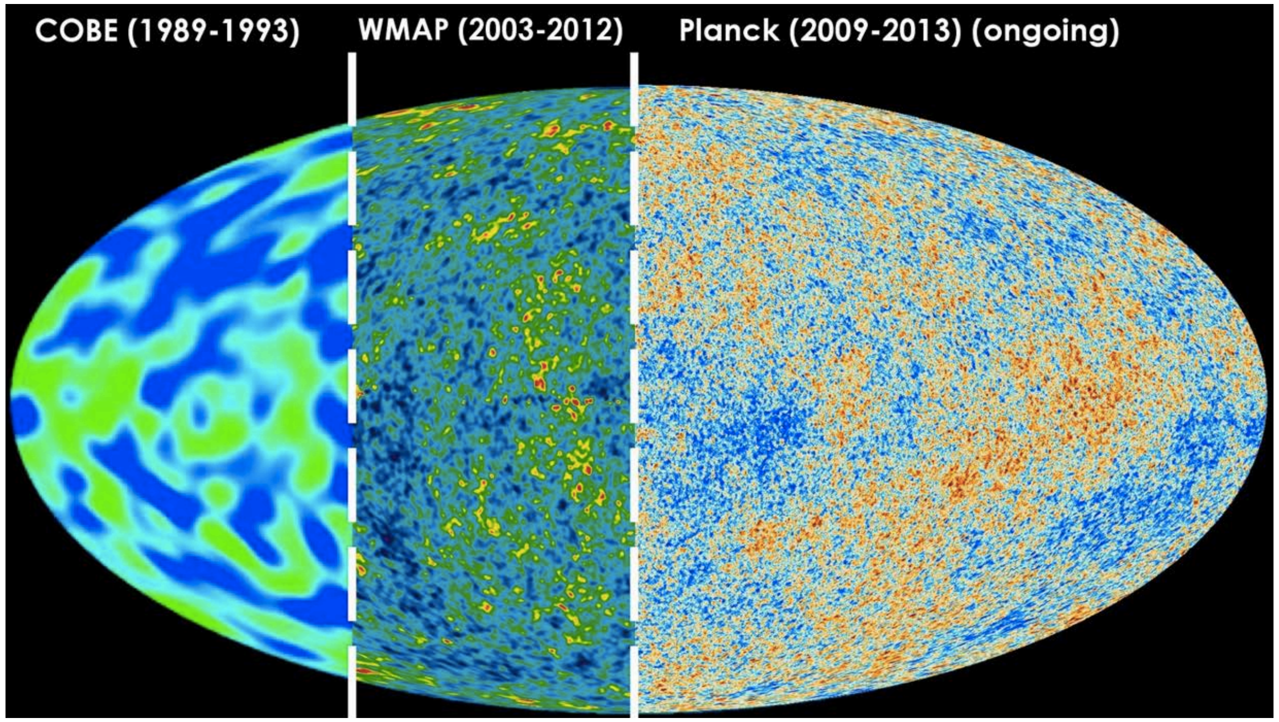

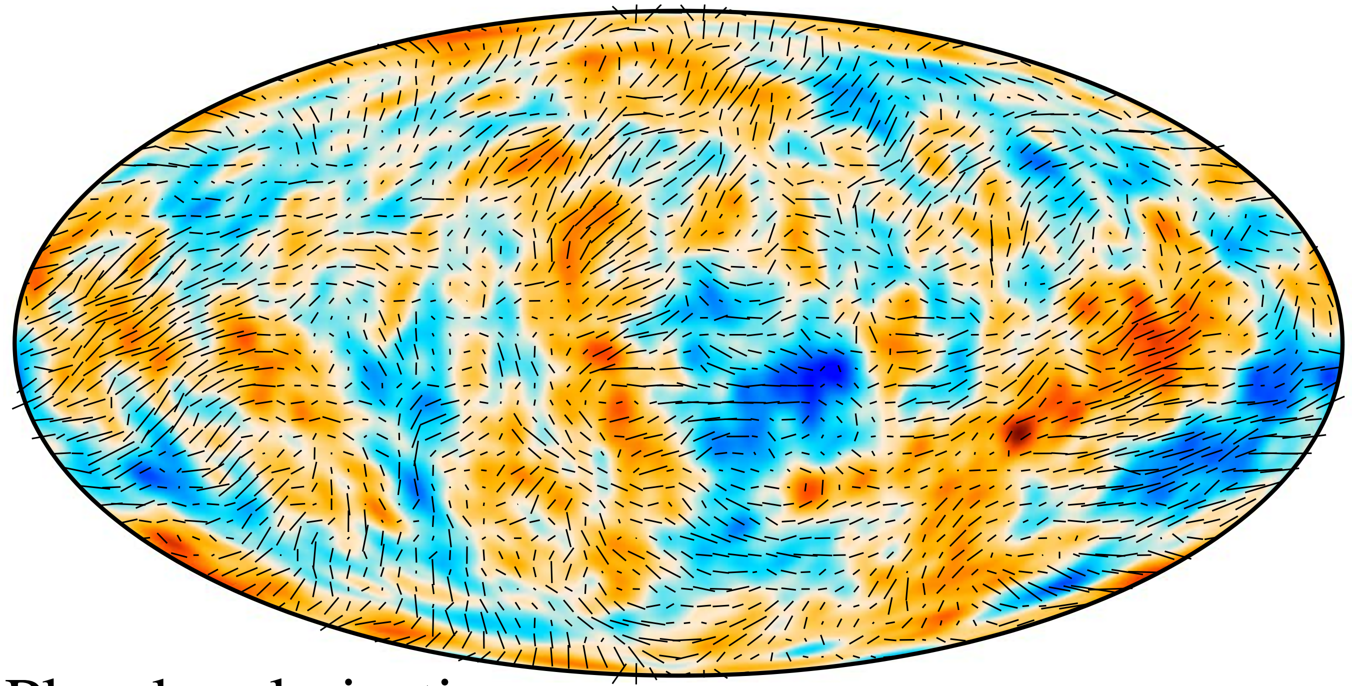

Planck polarization

The CMB success story

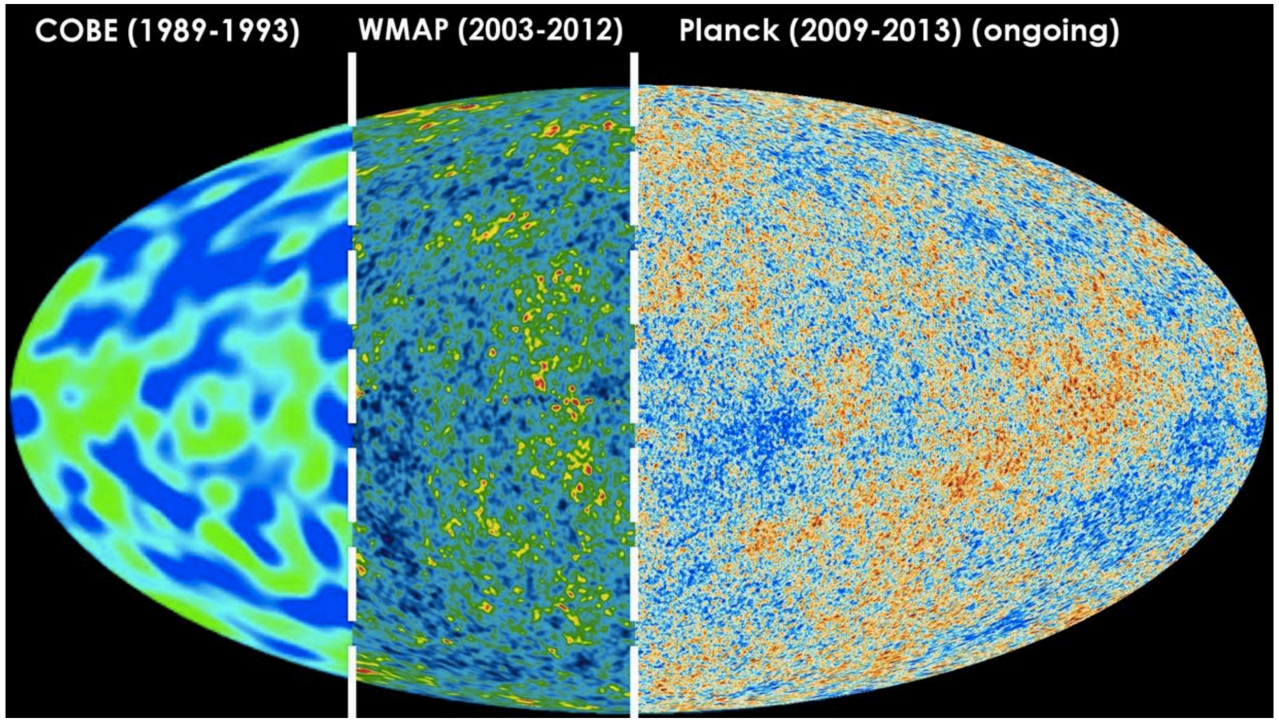

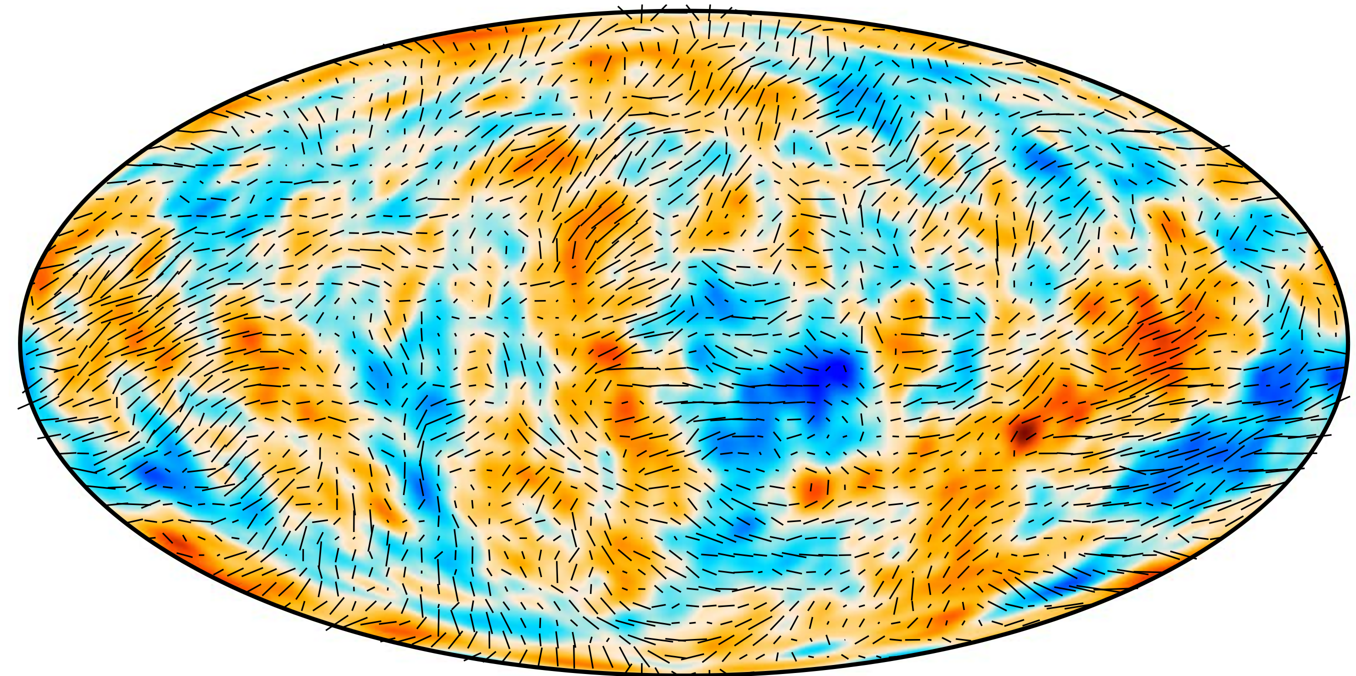

Planck polarization

Parameter	Plik [1]
$\Omega_b h^2$	0.02237 ± 0.00015
$\Omega_c h^2$	0.1200 ± 0.0012
$100\theta_{MC}$	1.04092 ± 0.00031
τ	0.0544 ± 0.0073
$\ln(10^{10} A_s)$	3.044 ± 0.014
n_s	0.9649 ± 0.0042

Planck collaboration 2018

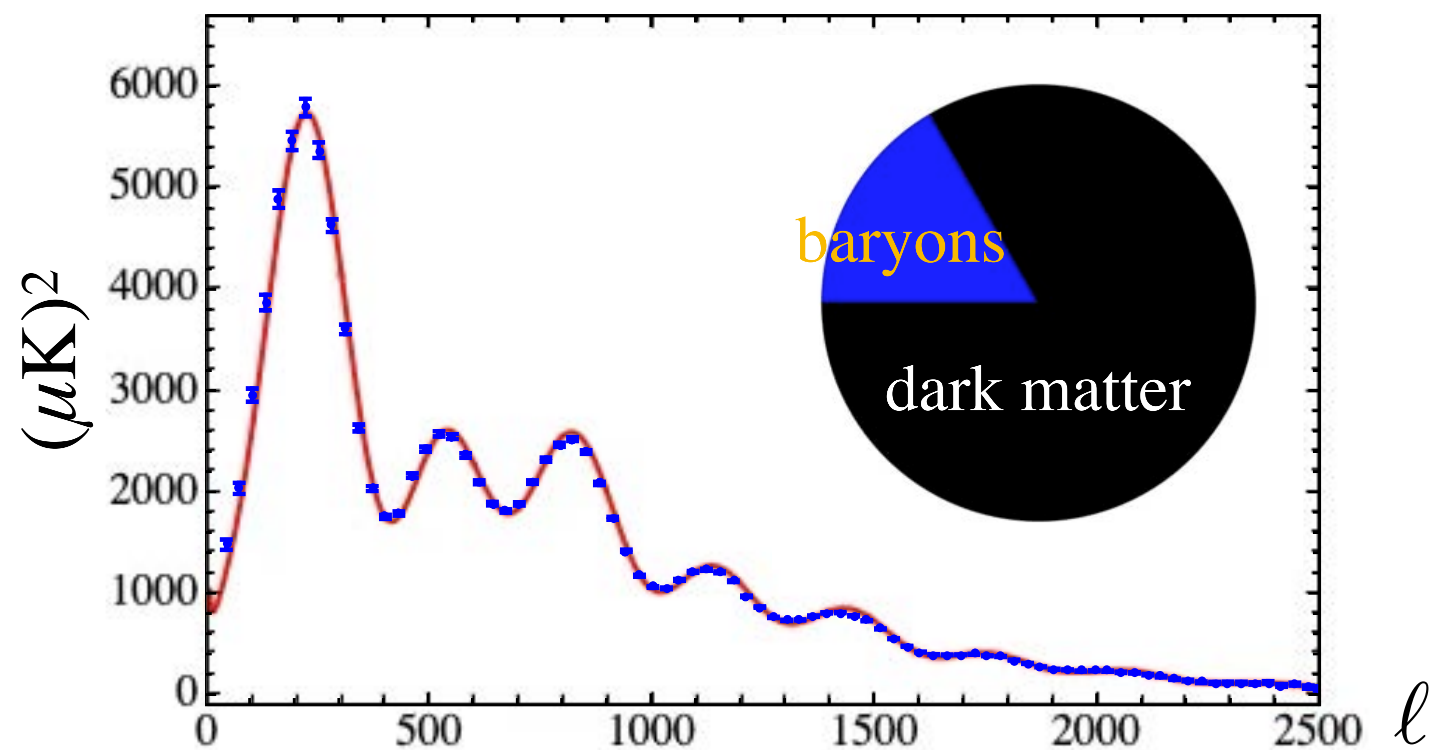

We are in the early days of gravitational-wave astronomy … and cosmology!

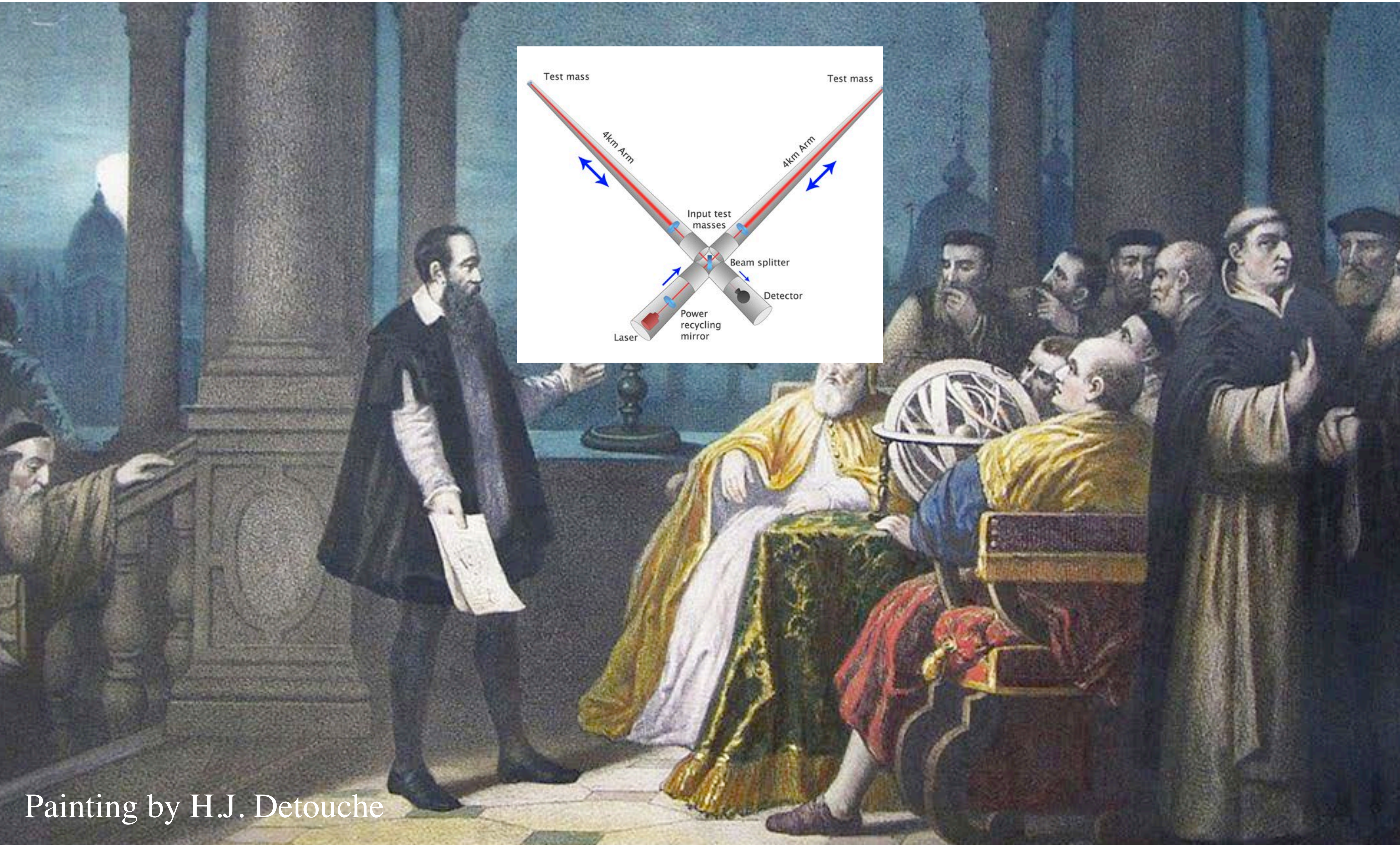

The gravitational-wave landscape

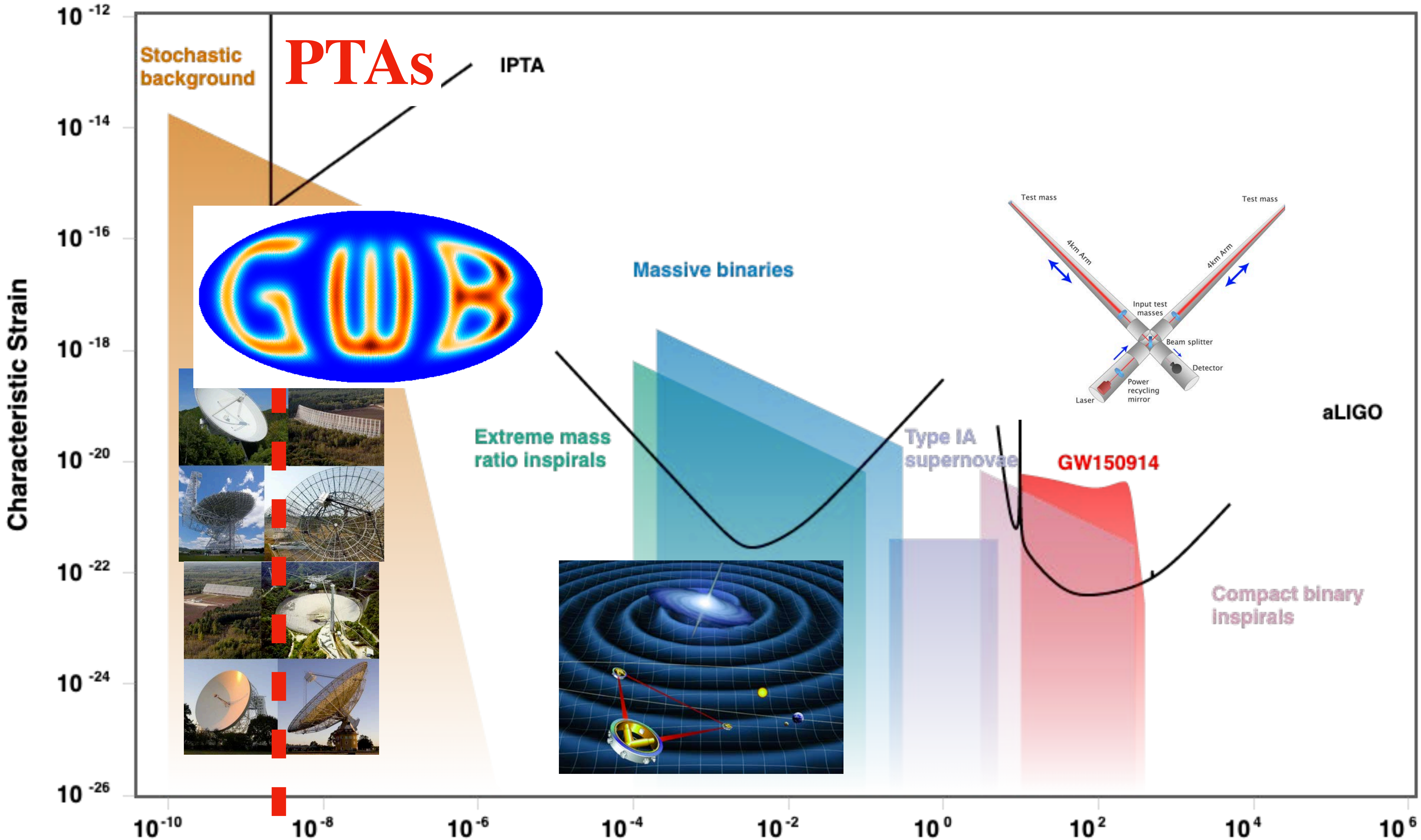

1/(10 yr) ≈ 3 nHz

made with gwplotter

Sources of nHz GWs

★ Inspiraling supermassive black hole binaries (SMBHBs).

Joint radiation of many circular SMBHBs leads to a **stochastic** GWB with characteristic strain

$$h_c(f) = A_{\mathrm{GWB}} \left(\frac{f}{\mathrm{yr}^{-1}} \right)^{-2/3}$$

$$A^2_{\mathrm{GWB}} \propto M^{5/3} \frac{dN_{\mathrm{remnants}}}{dV}$$

Phinney 2001

★``Primordial'' GWs, either ``truly primordial'', or sourced at second-order by scalar perturbations ($k \sim$ 1e6 Mpc^{-1}).

★"Exotica", e.g. cosmic strings

Status of PTAs

First step: set constraints on one single number, characteristic GW strain amplitude, assuming an isotropic stochastic GWB with specific frequency dependence

$$h_c(f) = h_c(1\ \mathrm{yr}^{-1})\,\left(f/\mathrm{yr}^{-1}\right)^{-\alpha}$$

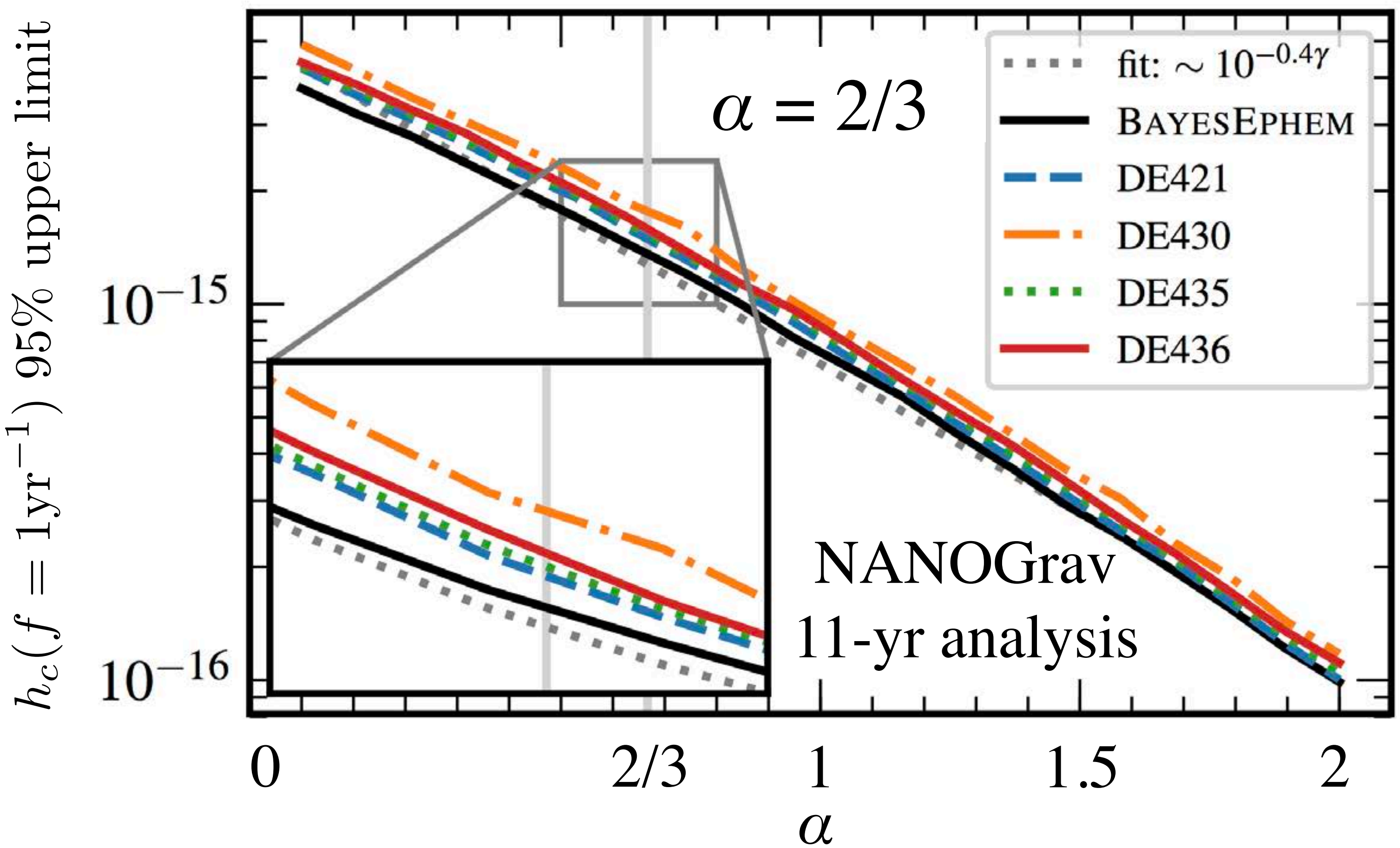

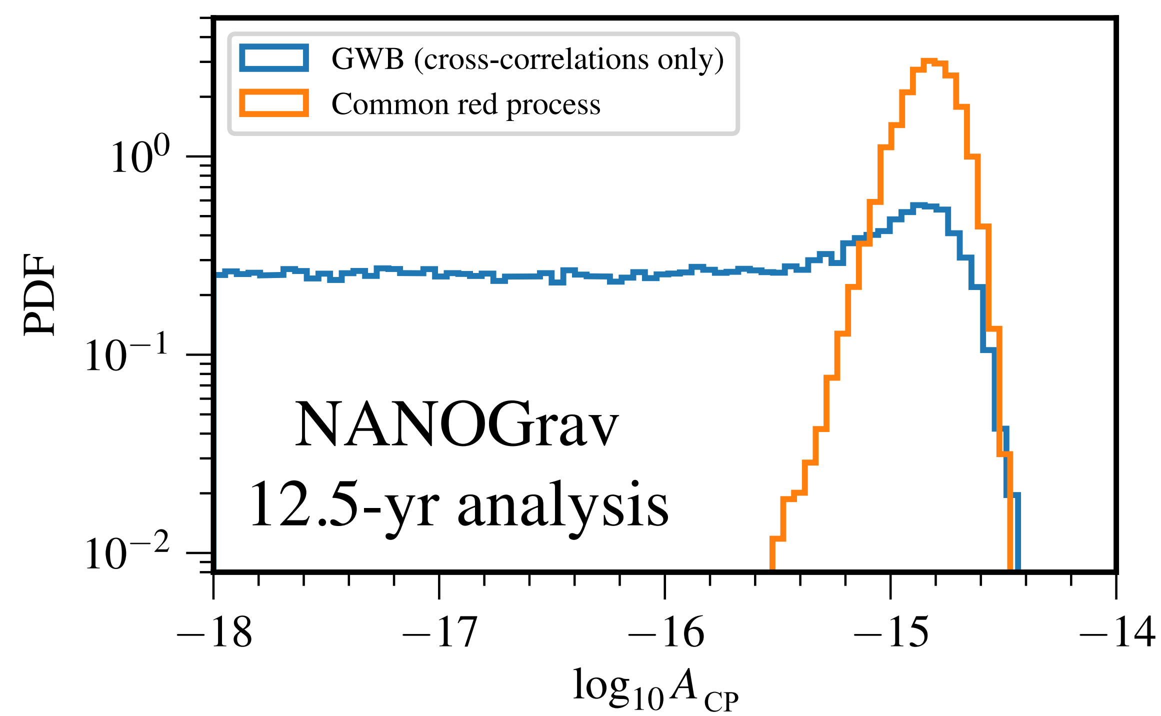

PTAs are still in the pre-Penzias & Wilson era

Looking ahead

- Frequency spectrum of the GWB ?

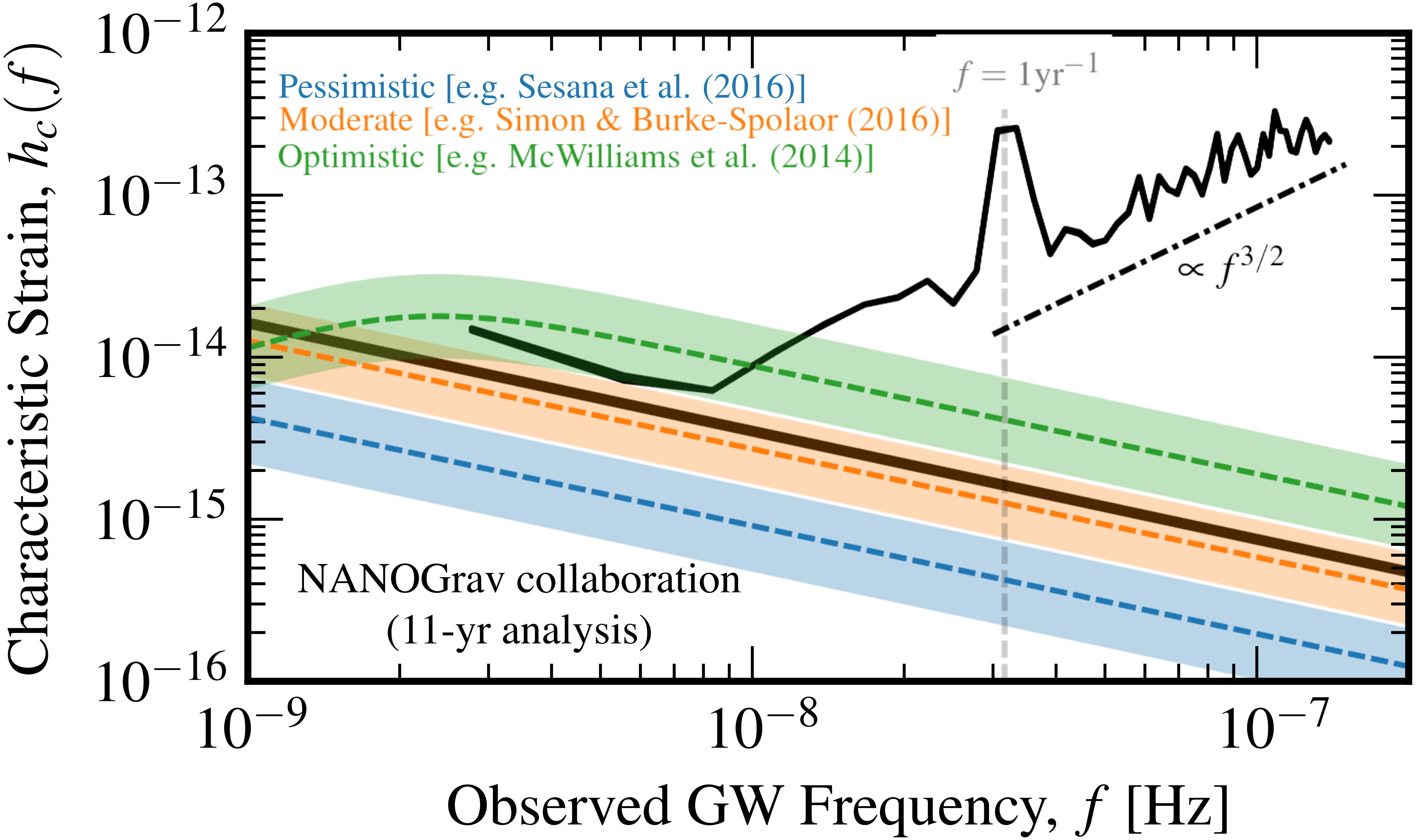

Looking ahead

- Anisotropies in GWB intensity?

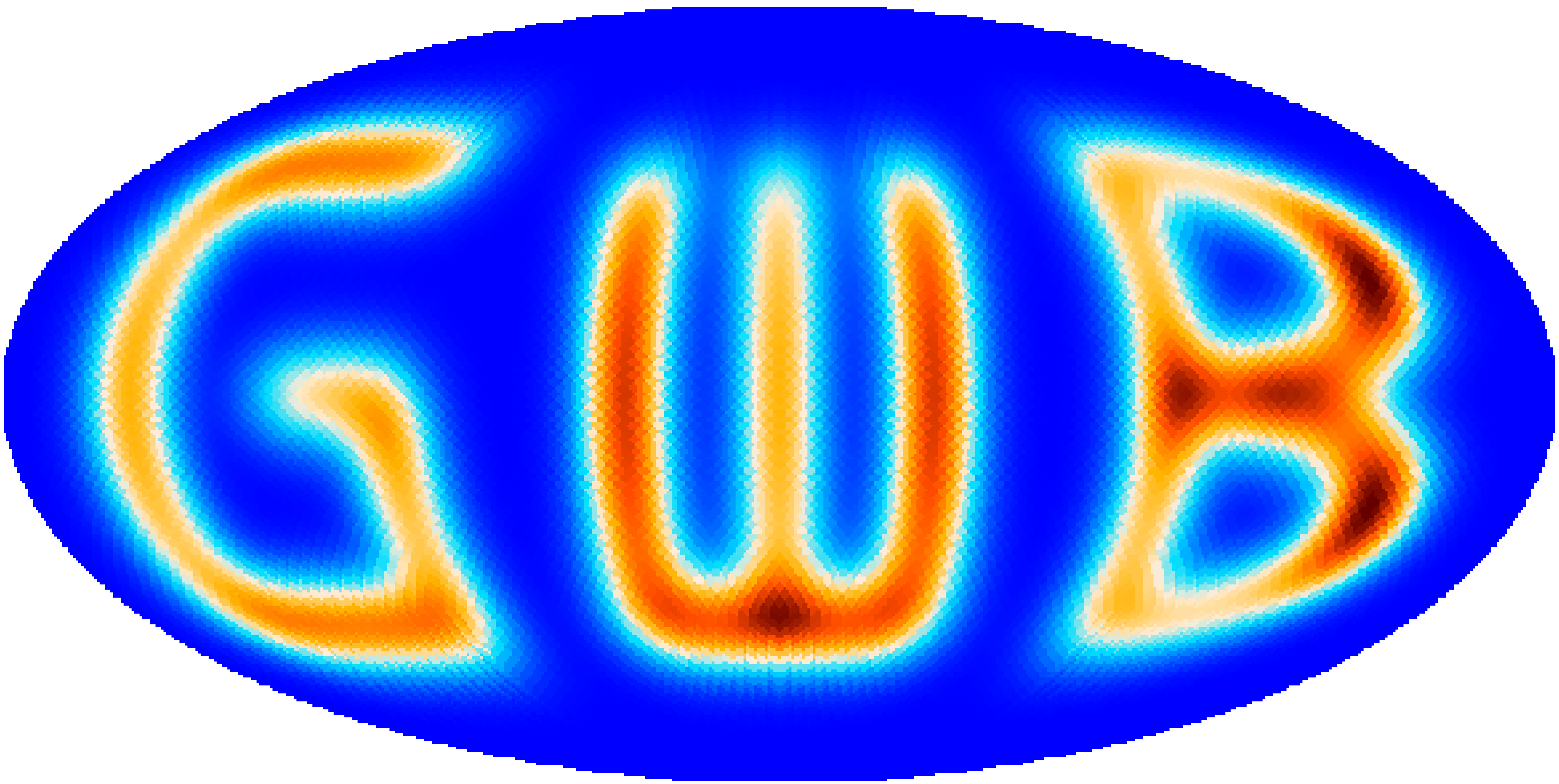

Anisotropies are **expected** from the Poisson statistics of finite number of SMBHBs (Mingarelli et al. 2013)

Looking ahead

- Polarization of the stochastic GWB?

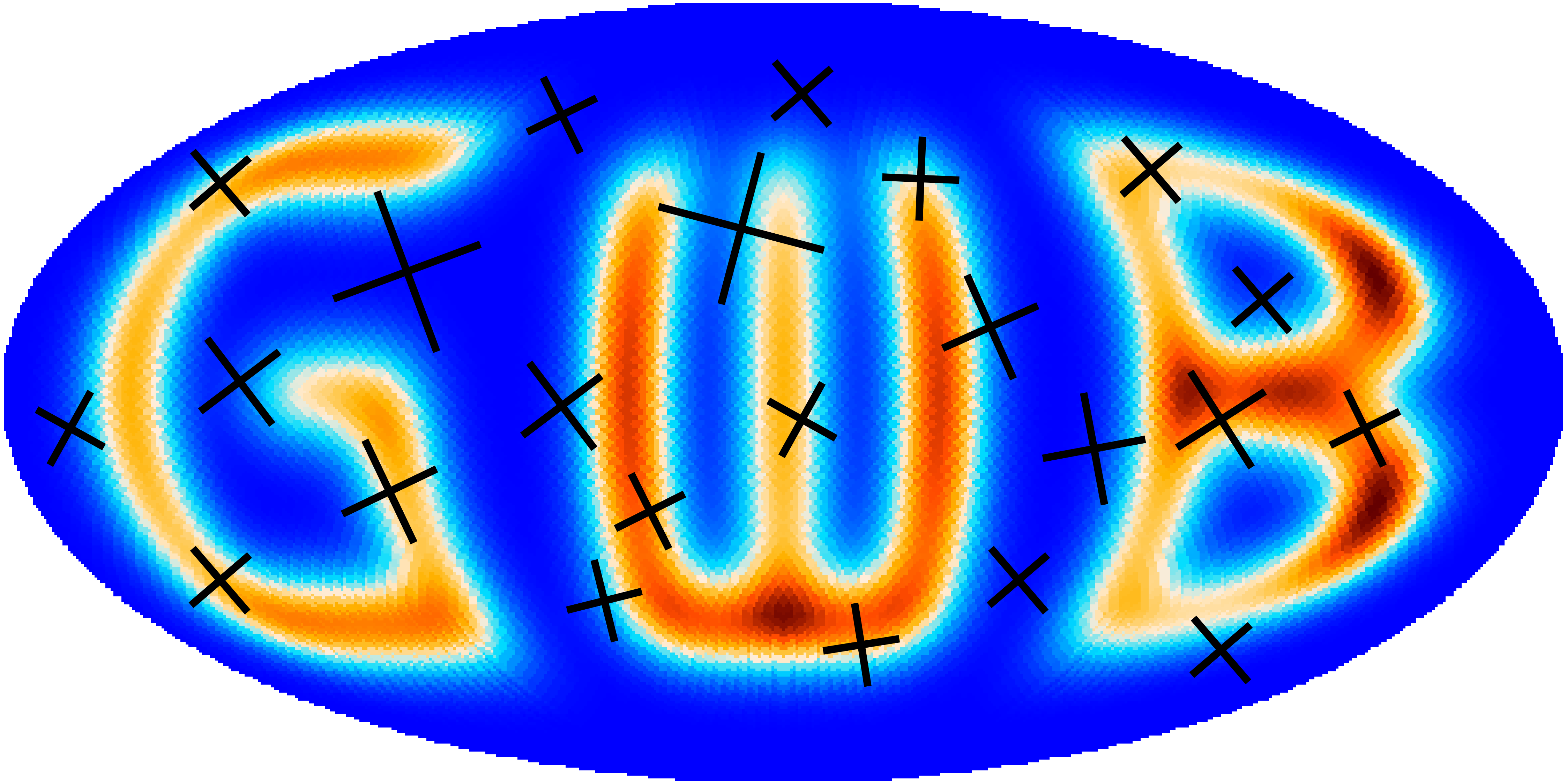

Looking ahead

=> What physics might we learn if and when we measure more properties of the GWB?

=> What can PTAs measure in the first place, and how well?

Why a Fisher formalism?

- Fisher formalism: ``theorist's reduction of the data analysis process".
- A detection of the gravitational-wave background can only be achieved with pulsar cross-correlations
- NANOGrav 12.5 year uses 45 pulsars, i.e. 990 pairs
- SKA promises hundreds of new millisecond pulsars, i.e. **tens of thousands of pairs**

➡ We need simple — but robust — tools to be able to make **forecasts** without running MCMCs, and to **guide** and **optimize** full-blown data analyses

Analogies and differences between EMWs and GWs

- Astrophysical sources always made of large numbers of incoherent microscopic emitters

=> Astrophysical EMWs are *always* ***stochastic*** (even "point sources")

direction of propagation

$$\hat{\Omega}_i E_i(f, \hat{\Omega}) = 0$$

=> 2 independent components

- Can detect deterministic GWs from single "microscopic" sources, e.g. a single binary.

- Superposition of many sources can lead to a **stochastic** GWB.

=> focus of this work

$$\hat{\Omega}_i h_{ij}(f, \hat{\Omega}) = 0$$

h_{ij} symmetric, trace-free

=> 2 independent components

Analogies and differences between EMWs and GWs

EMWs	GWs
$\langle E_i(f,\hat{\Omega})E_j^*(f,\hat{\Omega})\rangle$	$\langle h_{ab}(f,\hat{\Omega})h_{cd}^*(f,\hat{\Omega})\rangle$
$= I(f,\hat{\Omega})\left(\delta_{ij} - \hat{\Omega}_i\hat{\Omega}_j\right)$	$= \mathcal{I}(f,\hat{\Omega})\mathfrak{I}_{abcd}(\hat{\Omega})$
$+ V(f,\hat{\Omega})\epsilon_{ijk}\hat{\Omega}_k$	$+ \mathcal{V}(f,\hat{\Omega})\mathfrak{V}_{abcd}(\hat{\Omega})$
$+ L_{ij}(f,\hat{\Omega})$	$+ \mathcal{L}_{abcd}(f,\hat{\Omega})$
symmetric and trace-free 2 independent linear polarizations	symmetric and trace-free in all pairs 2 independent linear polarizations

Pulsar timing basics

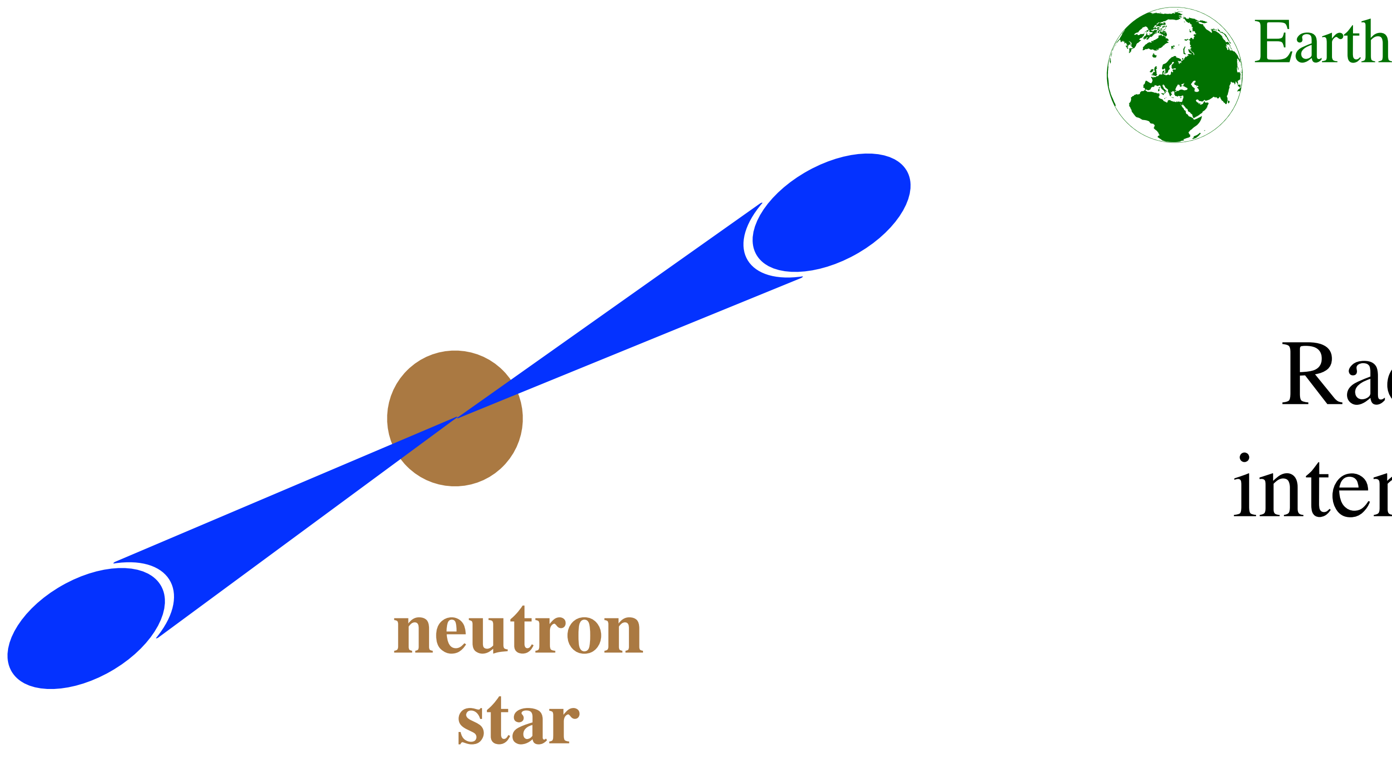

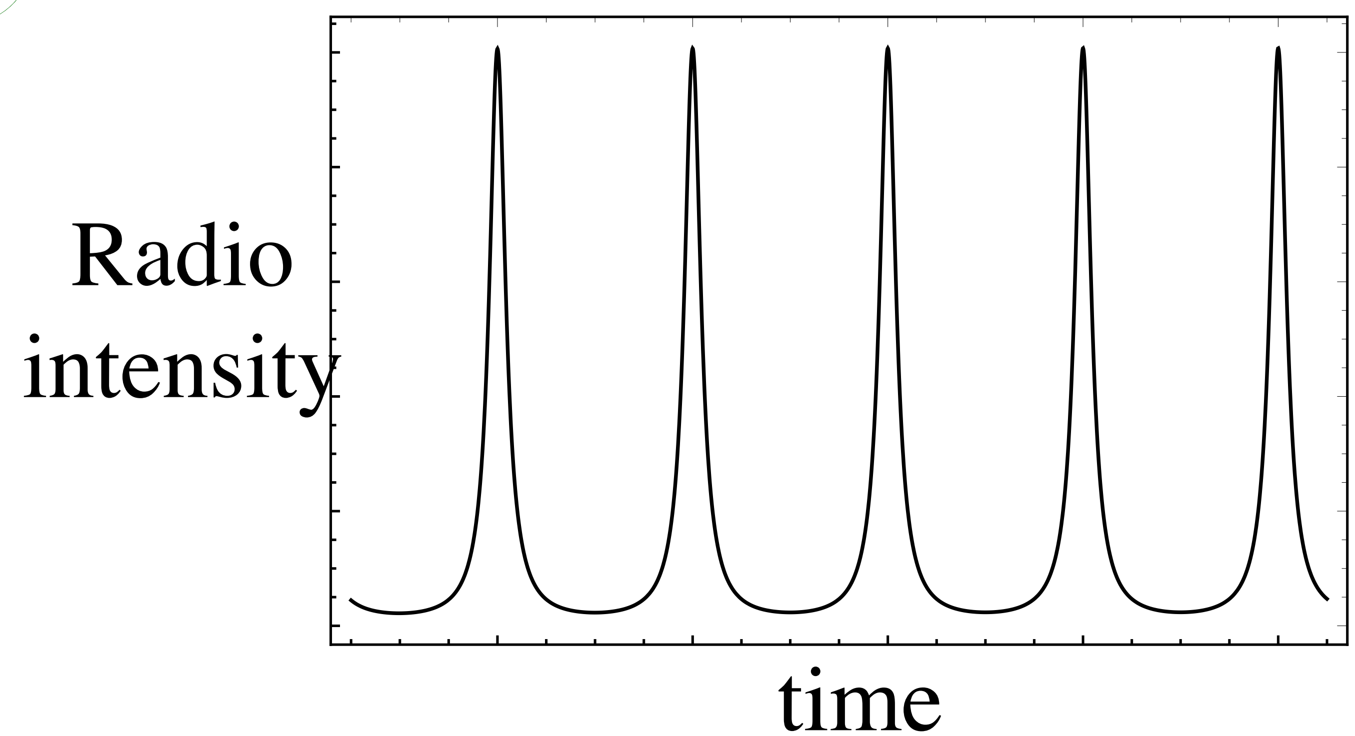

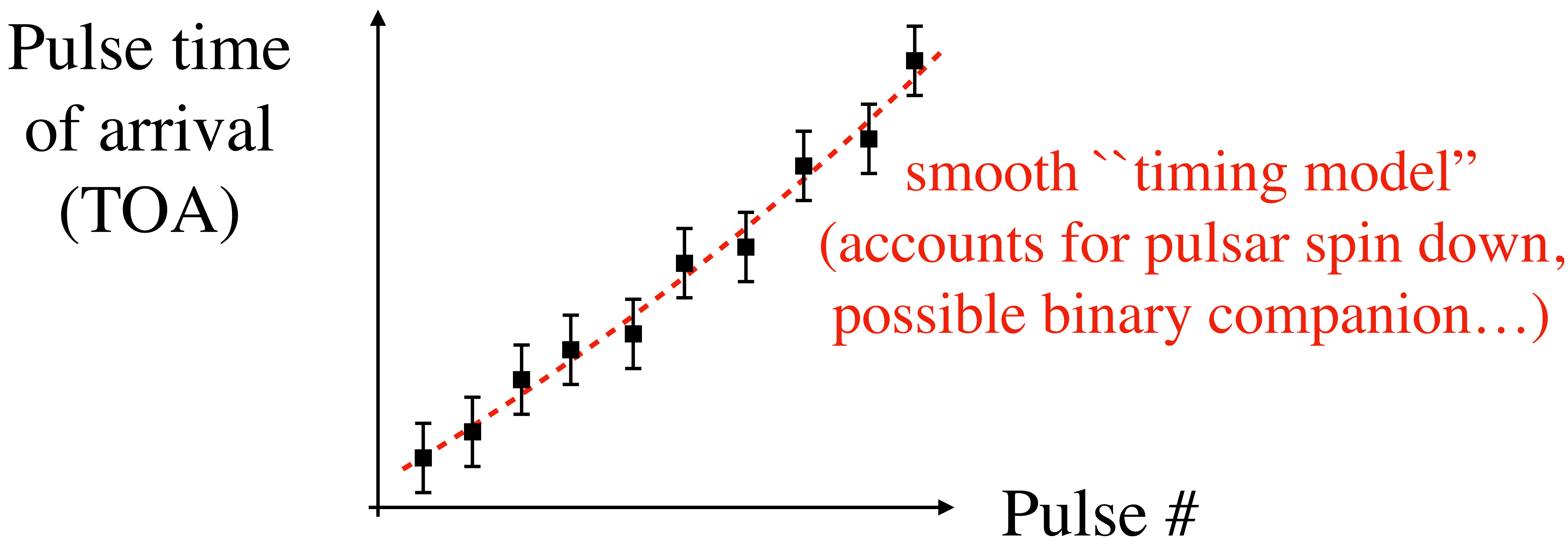

For each pulsar p: Time residual $R_p(t)$ = TOA - timing model(t)

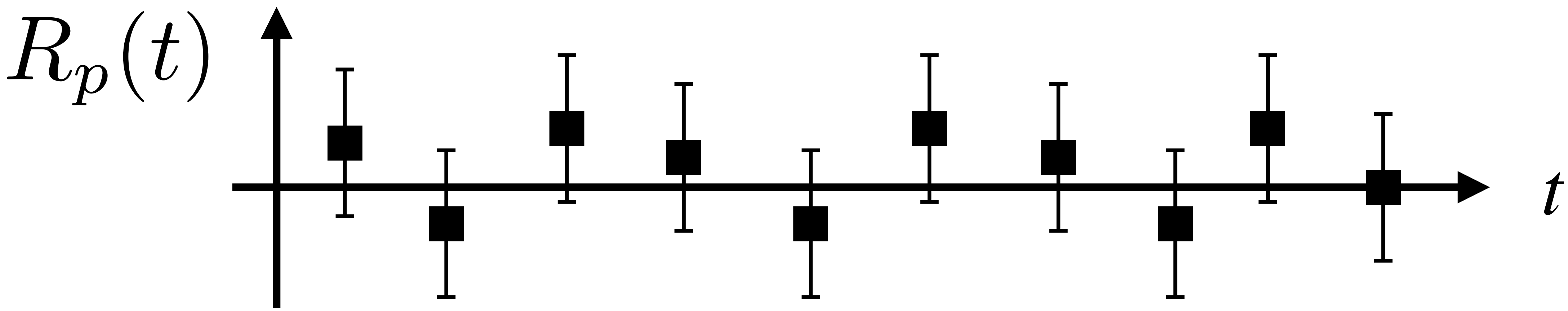

Real-life example: J1012+5307 (NANOGrav 12.5-yr data)

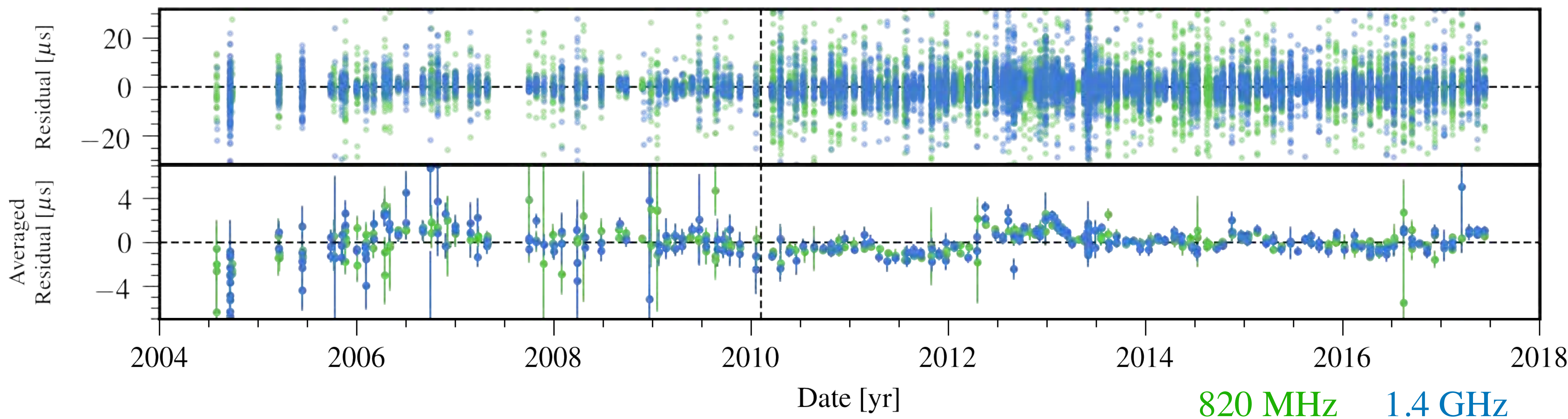

Fourier transform $R_p(t) \rightarrow R_p(f)$

Main sources of timing residuals

- Intrinsic pulsar noise.

$$\langle R_p^{\mathrm{int}}(f) R_q^{*\mathrm{int}}(f) \rangle = \sigma_p^2(f)\ \delta_{pq}$$

uncorrelated between different pulsars

- GW-induced timing residuals

$$R_p^{\mathrm{GW}}(f) = \frac{\hat{p}^a \hat{p}^b}{4\pi i f} \int d^2\hat{\Omega}\ \frac{h_{ab}(f,\hat{\Omega})}{(1+\hat{\Omega}\cdot\hat{p})}$$

$\hat{\Omega}$ = direction of GW propagation

Correlation of GW-induced residuals

$$\langle R_p^{\rm GW}(f) R_q^{*\rm GW}(f) \rangle = \mathcal{R}_{pq}^{\rm GW}(f)$$

$$\boxed{\mathcal{R}_{pq}^{\rm GW}(f) = \frac{1}{(4\pi f)^2} \int \frac{d^2\hat{\Omega}}{4\pi} \gamma_{\hat{p}\hat{q}}(\hat{\Omega}) \mathcal{I}(f, \hat{\Omega})}$$

$$\gamma_{pq}(\hat{\Omega}) \equiv 2 \frac{\left(\hat{p}\cdot\hat{q} - (\hat{p}\cdot\hat{\Omega})(\hat{q}\cdot\hat{\Omega})\right)^2}{(1+\hat{p}\cdot\hat{\Omega})(1+\hat{q}\cdot\hat{\Omega})} - (1-\hat{p}\cdot\hat{\Omega})(1-\hat{q}\cdot\hat{\Omega})$$

pairwise timing response function

$$\mathcal{R}_{pq}^{\rm GW}(f) = \frac{\boldsymbol{\gamma}_{\hat{p}\hat{q}} \cdot \boldsymbol{\mathcal{I}}(f)}{(4\pi f)^2}$$

$$\boxed{\boldsymbol{M}_1 \cdot \boldsymbol{M}_2 \equiv \int \frac{d^2\hat{\Omega}}{4\pi} M_1(\hat{\Omega}) M_2(\hat{\Omega})}$$

For an *isotropic* GWB: $\mathcal{I}(f,\hat{\Omega}) = \mathcal{I}(f)$

$$\mathcal{R}^{\mathrm{GW}}_{pq}(f) = \frac{\mathcal{I}(f)}{(4\pi f)^2} \boxed{\int \frac{d^2\hat{\Omega}}{4\pi} \gamma_{\hat{p}\hat{q}}(\hat{\Omega})}$$

$\mathcal{H}(\hat{p}\cdot\hat{q})$

Hellings & Downs curve

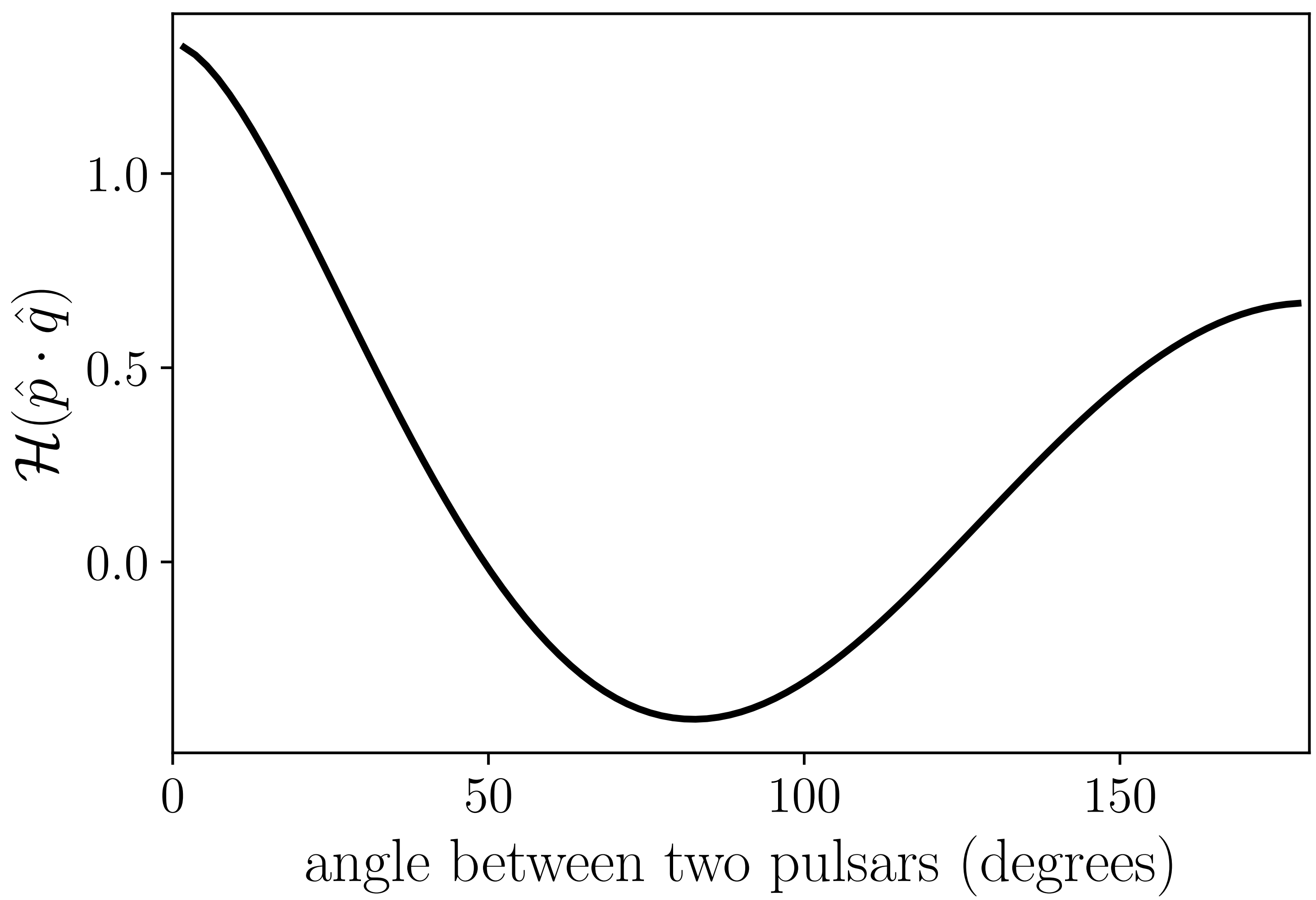

Constructing the Fisher "matrix"

- Construct **quadratic estimators** for timing residual cross-power spectra, for each pair $(p, q), p \neq q$

$$\widehat{\mathcal{R}}_{pq}(f) \qquad [\leftrightarrow \hat{C}_\ell = \frac{1}{2\ell+1}\sum_m |a_{\ell m}|^2 \ \text{ for CMB}]$$

- Approximate distribution of estimators as Gaussian. Compute covariance in weak-signal limit.

Translates to a **Gaussian likelihood for GWB intensity**, given timing residual data.

Constructing the Fisher "matrix"

Effective noise strain for each pulsar:

$$h_{c,p}^2(f) \equiv \frac{4}{3}\frac{(4\pi f)^2\sigma_p^2(f)}{\mathcal{T}_p(f)}$$

Loss of information at low frequencies when fitting a smooth timing model

(Blandford, Narayan & Romani 1984)

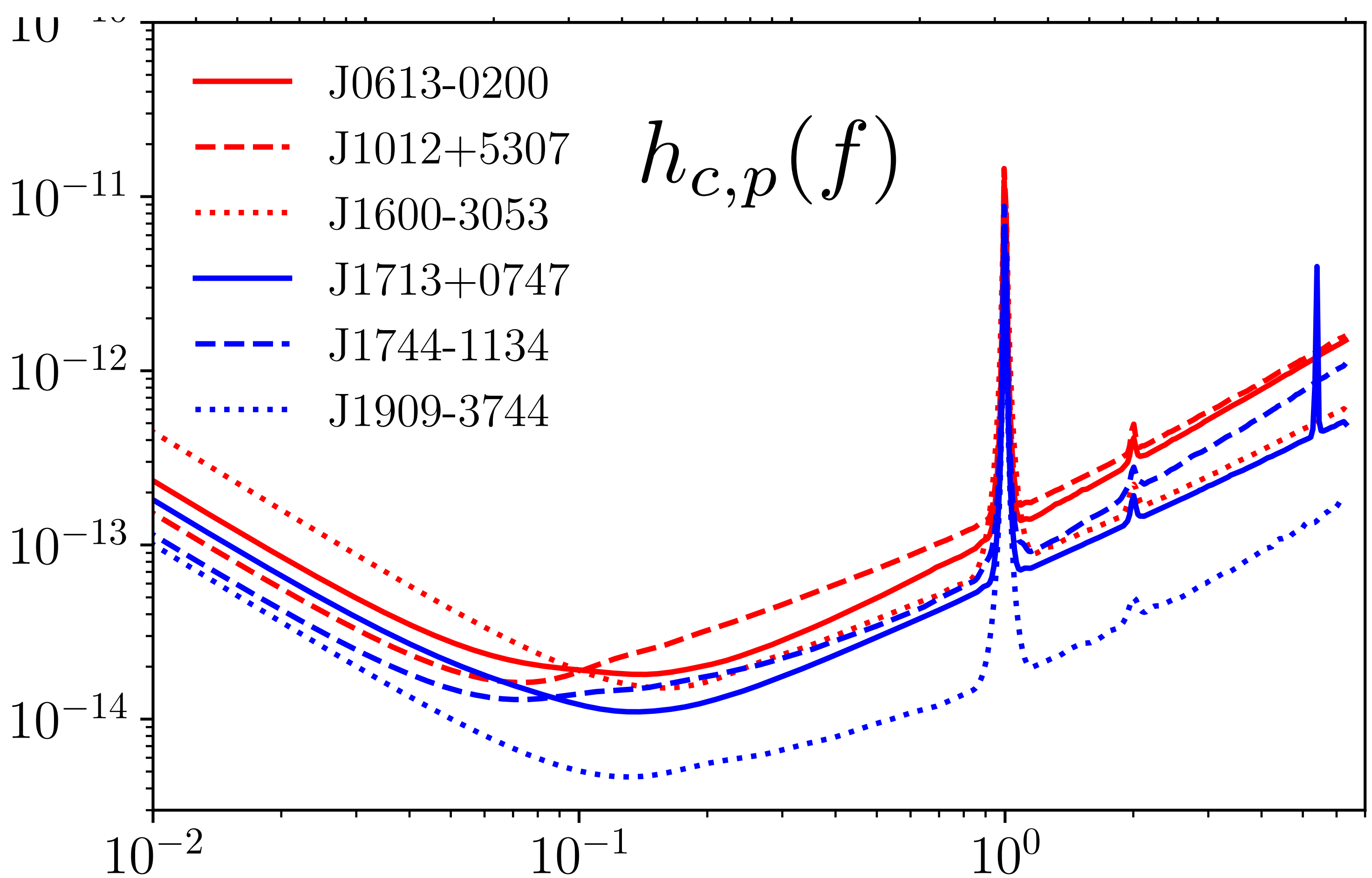

Computed with **Hasasia** (Hazboun, Romano & Smith 2019)

Only requires analyzing single pulsars (no cross correlations involved)

Constructing the Fisher "matrix"

Special case: factorized frequency and angular dependence.

$$\mathcal{I}(f,\hat{\Omega}) = \mathcal{A}(\hat{\Omega})\left(f/\mathrm{yr}^{-1}\right)^{-2\alpha}$$

$$\mathcal{L}[\boldsymbol{\mathcal{A}}|\mathrm{data}] \propto \exp\left[-\frac{1}{2}(\boldsymbol{\mathcal{A}}-\widehat{\boldsymbol{\mathcal{A}}})\cdot\boldsymbol{\mathcal{F}}\cdot(\boldsymbol{\mathcal{A}}-\widehat{\boldsymbol{\mathcal{A}}})\right]$$

$$\mathcal{F}(\hat{\Omega},\hat{\Omega}') = \sum_{p\neq q} \mathcal{F}_{pq}\,\gamma_{pq}(\hat{\Omega})\,\gamma_{pq}(\hat{\Omega}')$$

noise properties

geometric properties

$$\mathcal{F}_{pq} \propto \int df\,\frac{\left(f/\mathrm{yr}^{-1}\right)^{-4\alpha}}{h_{c,p}^2(f)h_{c,q}^2(f)}$$

Warmup: idealized PTA

Consider an idealized PTA with $N_{\rm psr} >> 1$ identical pulsars distributed isotropically on the sky

$$\mathcal{F}(\hat{\Omega}, \hat{\Omega}') \propto F(\hat{\Omega}, \hat{\Omega}') \equiv \frac{1}{N_{\rm pair}} \sum_{p \neq q} \gamma_{\hat{p}\hat{q}}(\hat{\Omega}) \gamma_{\hat{p}\hat{q}}(\hat{\Omega}')$$

$$\boldsymbol{F}(\hat{\Omega}, \hat{\Omega}') \underset{N_{\rm psr} \to \infty}{\longrightarrow} \mathcal{F}_\infty(\hat{\Omega} \cdot \hat{\Omega}')$$

$$\mathcal{F}_\infty(\chi) = \frac{16}{9(1+\chi)^2} \left[\left(\frac{1-\chi^2}{4} + 2 - \chi + 3 \frac{1-\chi}{1+\chi} \log \frac{1-\chi}{2} \right)^2 + \left(2 - \chi + 3 \frac{1-\chi}{1+\chi} \log \frac{1-\chi}{2} \right)^2 \right]$$

Warmup: idealized PTA

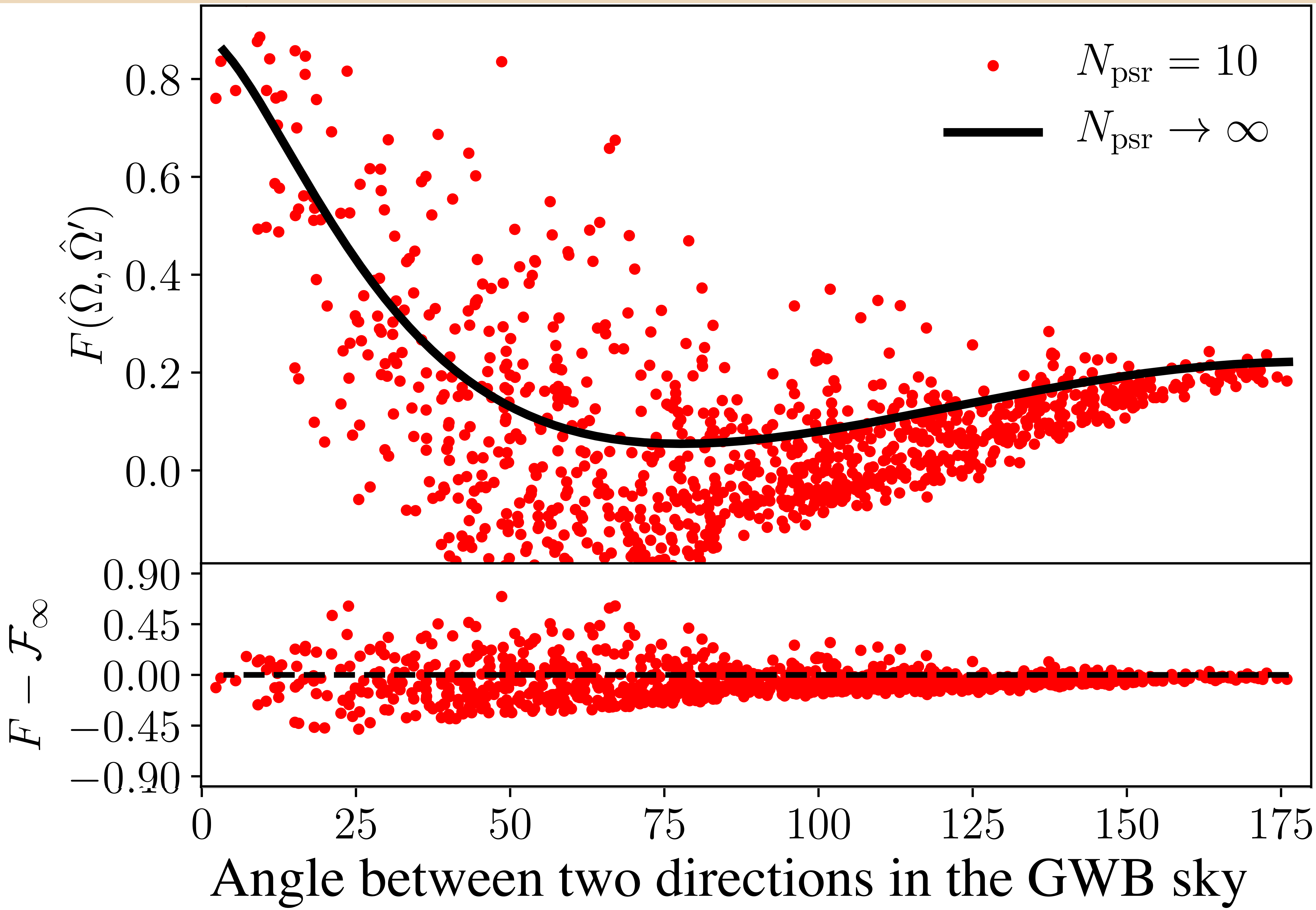

Warmup: idealized PTA

$$\mathcal{F}_\infty(\hat{\Omega}\cdot\hat{\Omega}') = \sum_\ell (2\ell+1)\mathcal{F}_\ell \; P_\ell(\hat{\Omega}\cdot\hat{\Omega}') = 4\pi \sum_{\ell,m} \mathcal{F}_\ell \; \mathcal{Y}_{\ell m}(\hat{\Omega})\mathcal{Y}_{\ell m}(\hat{\Omega}')$$

=> The spherical harmonics are the eigenmaps of the idealized PTA Fisher matrix for $N_{\rm psr} \to \infty$

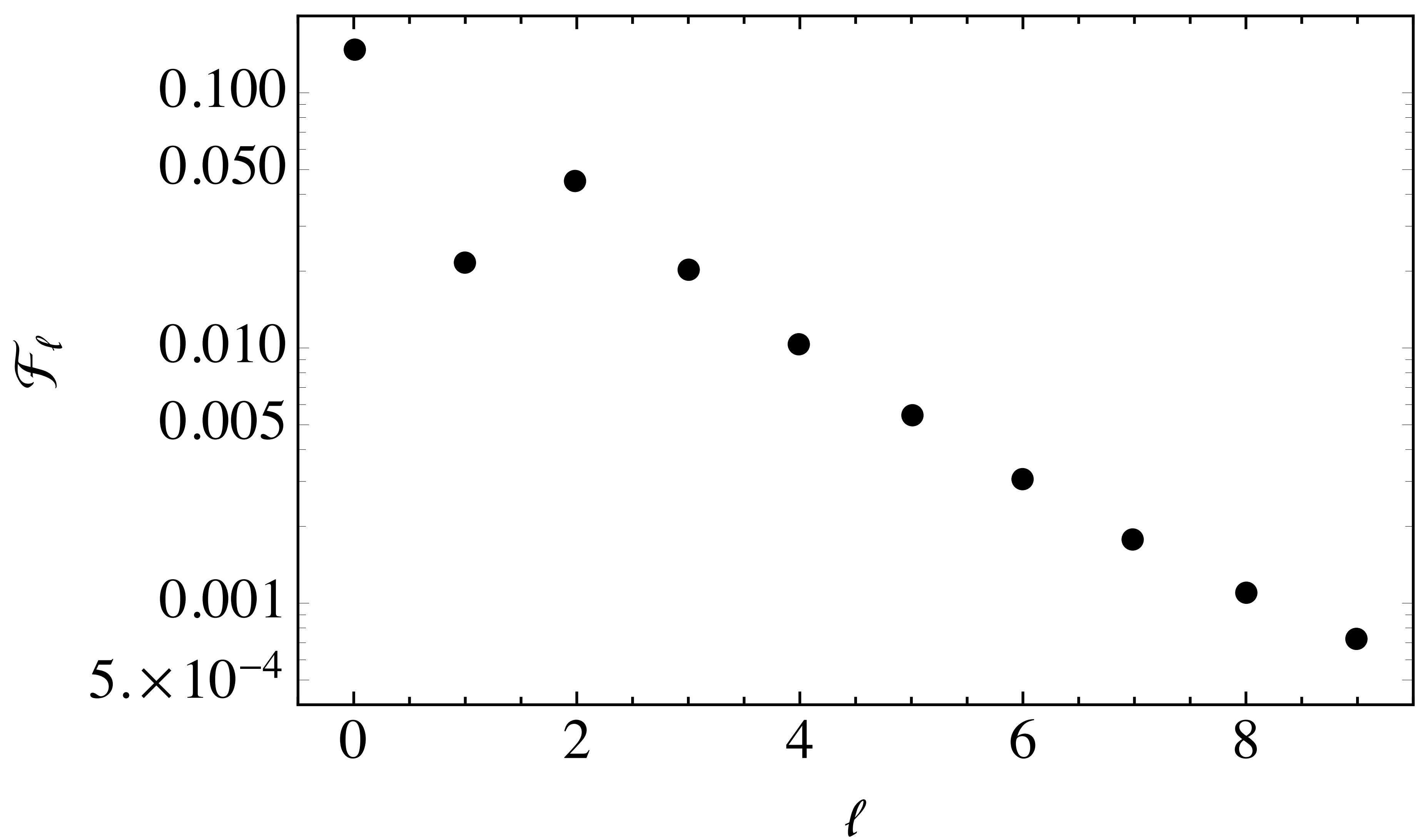

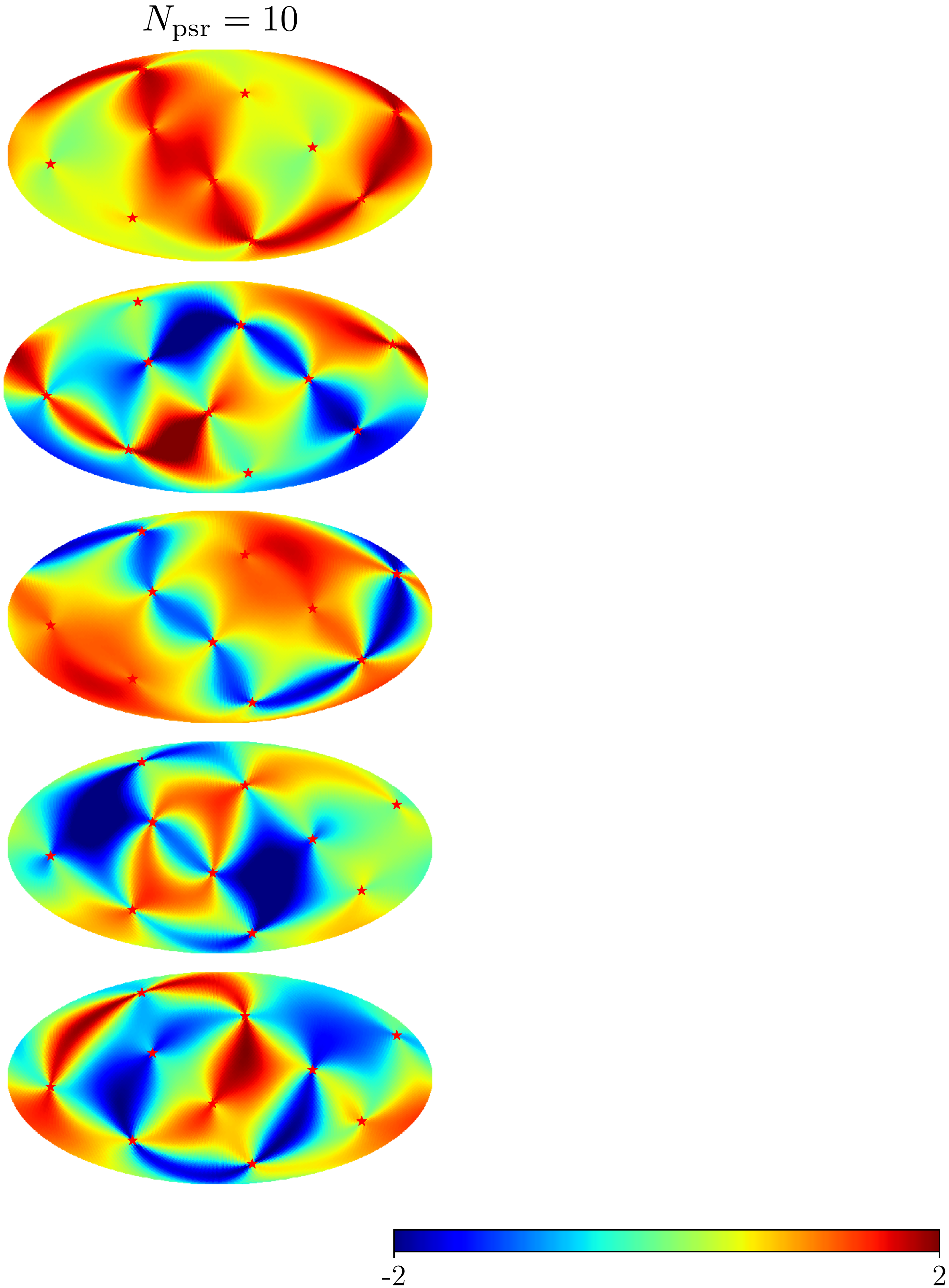

$N_{\rm psr} = 10$
-2
2

Warmup: idealized PTA

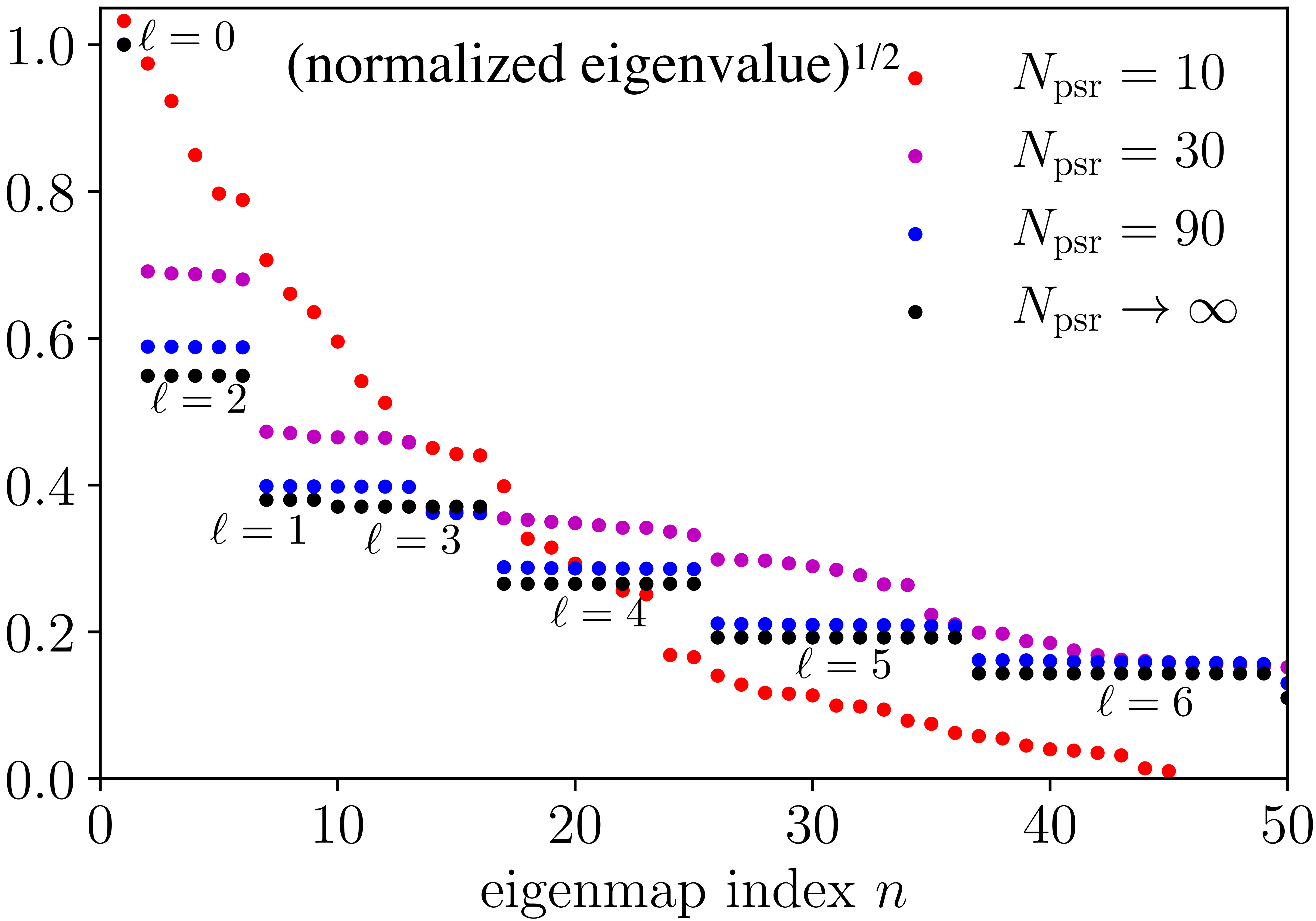

Application to the EPTA

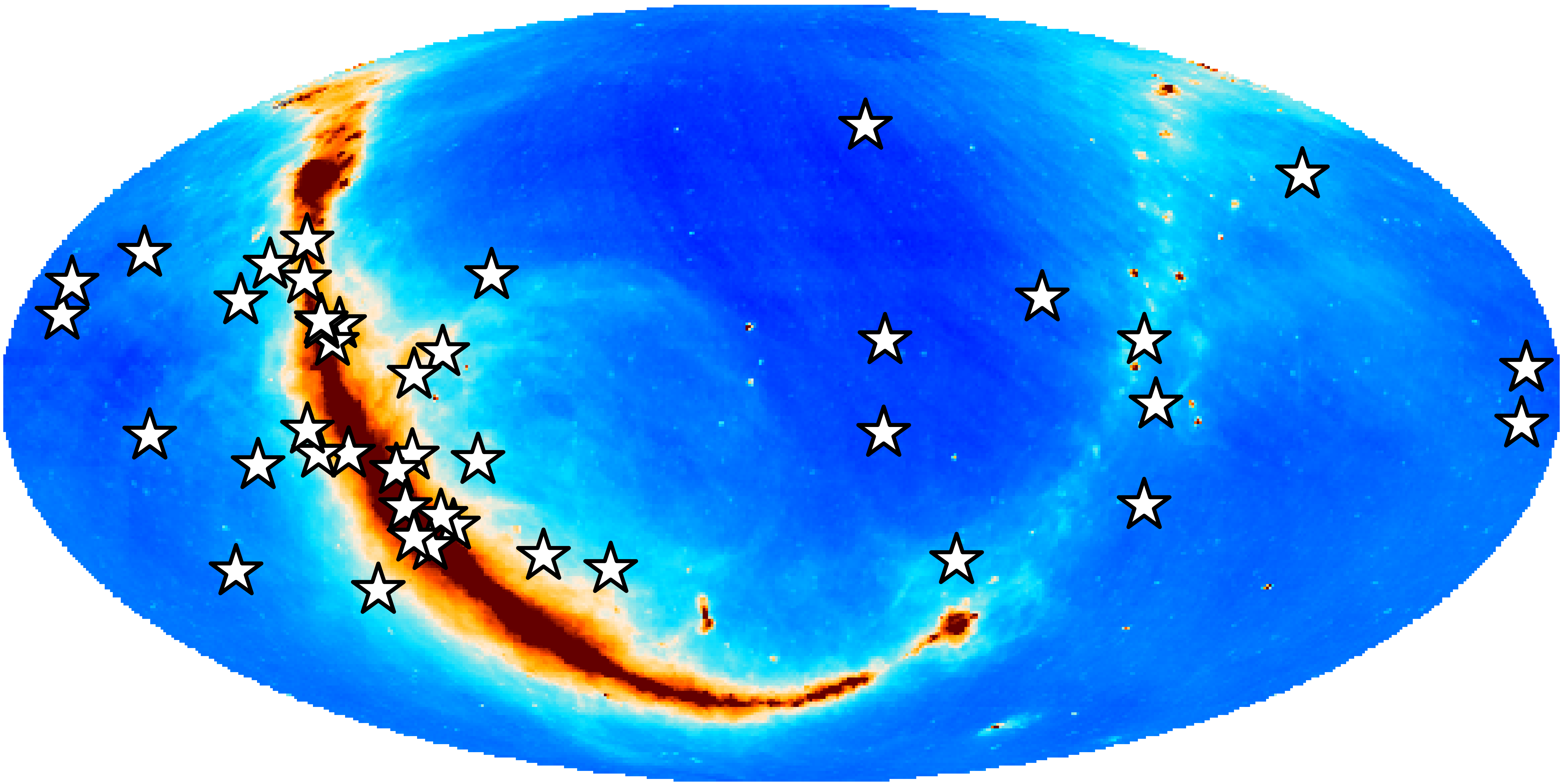

42 pulsars, timed for up to 17 years

Application to the EPTA

Characteristic noise strains obtained by analyzing residuals of each pulsar separately (no cross-correlation required)

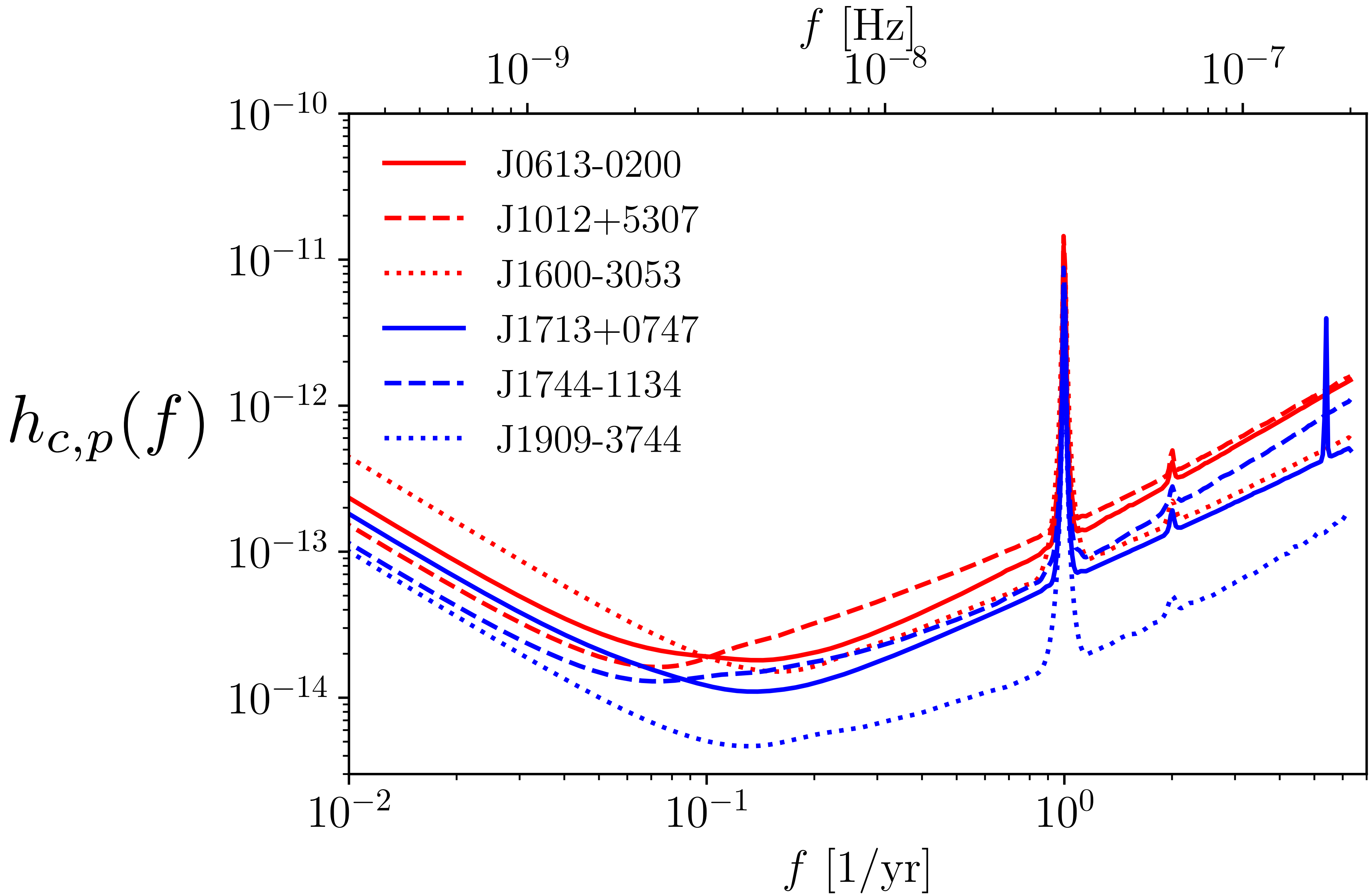

Warmup: monopole sensitivity

Signal-to-noise ratio of a given GWB amplitude:

$$\mathrm{SNR}^2 = \boldsymbol{\mathcal{A}} \cdot \boldsymbol{\mathcal{F}} \cdot \boldsymbol{\mathcal{A}} = \sum_{p \neq q} \mathcal{F}_{pq} \left[\boldsymbol{\gamma}_{\hat{p}\hat{q}} \cdot \boldsymbol{\mathcal{A}} \right]^2$$

Apply to a pure monopole: $\mathcal{A}(\hat{\Omega}) = A^2_{\mathrm{GWB}}$

$$\boldsymbol{\gamma}_{\hat{p}\hat{q}} \cdot \boldsymbol{\mathcal{A}} = A^2_{\mathrm{GWB}} \mathcal{H}(\hat{p} \cdot \hat{q})$$

Hellings & Downs curve

$$\mathrm{SNR}^2 = A^4_{\mathrm{GWB}} \sum_{p \neq q} \mathcal{F}_{pq} \left[\mathcal{H}(\hat{p} \cdot \hat{q}) \right]^2$$

$$\Rightarrow \quad \boxed{\text{sensitivity: } \; A^{95\%}_{\mathrm{GWB}} \; \text{ such that } \; \mathrm{SNR} = 2}$$

Application to 6 EPTA pulsars

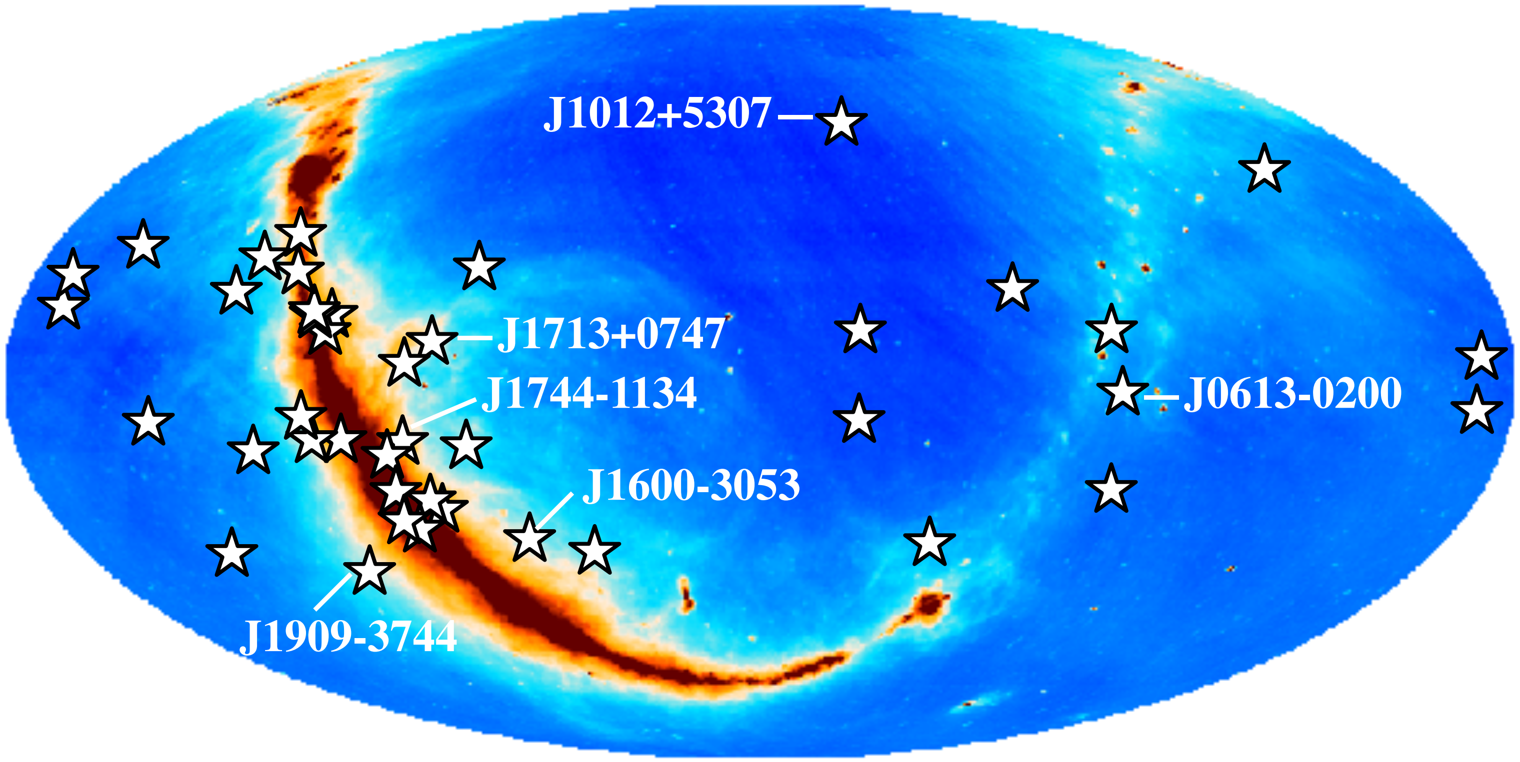

Were found to be the best pulsars for **continuous wave searches**

- We find a 2-σ sensitivity $\quad A^{95\%}_{\mathrm{GWB}} \approx 3.4 \times 10^{-15}$

- Compare with EPTA collaboration 95% upper limits of 3.0e-15 (Lentati et al. 2015) and 3.9e-15 (Taylor et al. 2015)

- With full EPTA array we estimate 95% sensitivity of 2.5e-15

Best pulsar **pairs** for monopole searches

$$\mathrm{SNR}^2 = A^4_{\mathrm{GWB}} \sum_{p \neq q} \mathcal{F}_{pq} \left[\mathcal{H}(\hat{p} \cdot \hat{q})\right]^2$$

SNR^2 contribution of each **pulsar pair**

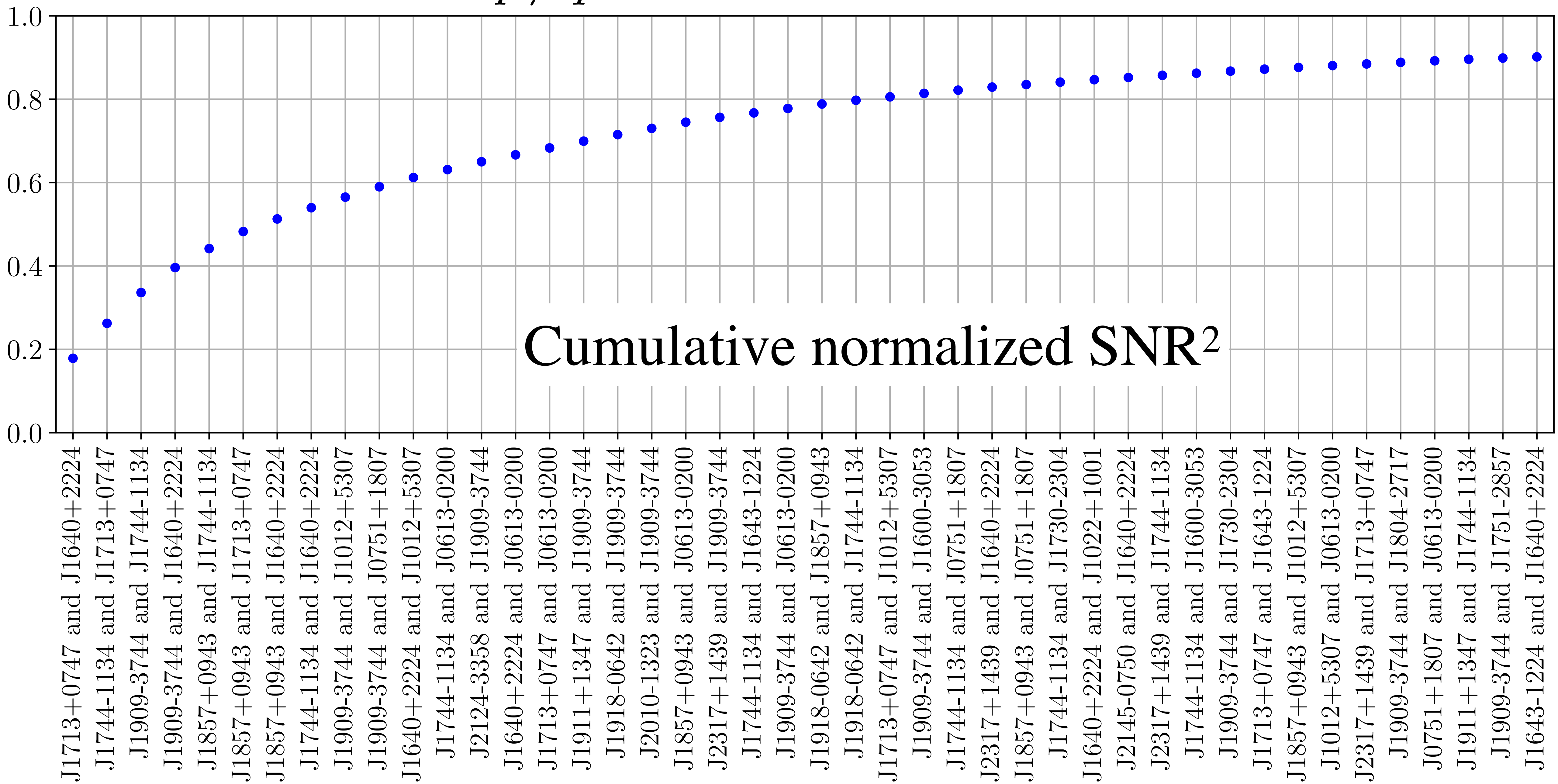

The 44 best pairs (out of 861) provide 90% of SNR^2

Beyond the monopole

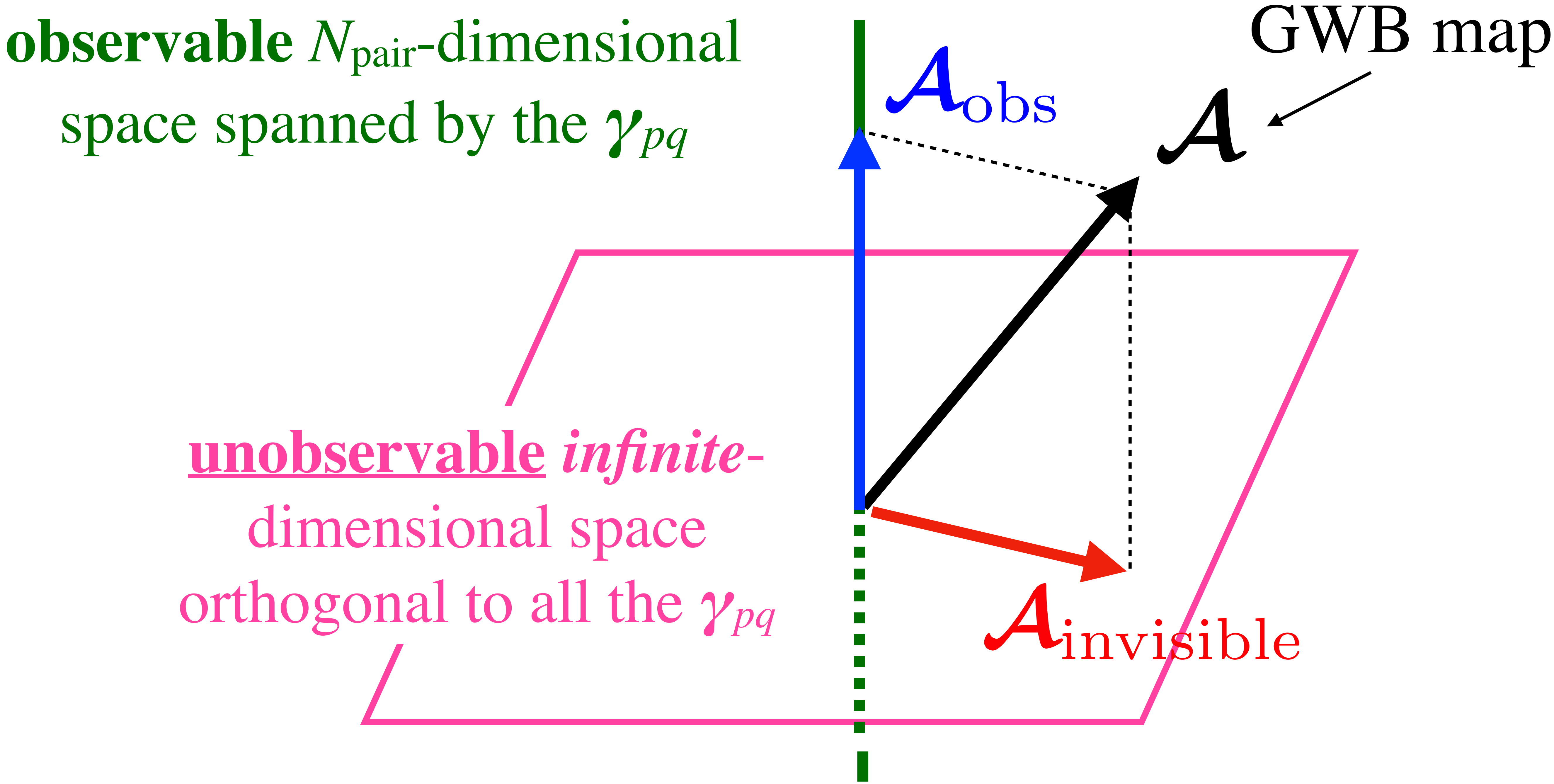

=> Can at most observe/ constrain N_{pair} independent components of the GWB angular dependence

Searching for anisotropies of known shape

Suppose we have good physical reasons to expect

$$\mathcal{A}(\hat{\Omega}) = \sum_{n=1}^{N_{\rm maps}} \mathcal{A}_n M_n(\hat{\Omega})$$

known basis maps

We want to estimate the sensitivity to the $\mathcal{A}_n$

only well defined if $N_{\mathbf{maps}} \leq N_{\mathbf{pair}}$

$$\text{cov}(\mathcal{A}_n, \mathcal{A}_m) = (F^{-1})_{nm} \qquad F_{nm} \equiv \boldsymbol{M}_n \cdot \boldsymbol{\mathcal{F}} \cdot \boldsymbol{M}_m$$

$$\mathcal{A}_n^{95\%} = 2\sqrt{\text{var}(\mathcal{A}_n)}$$

Example 1: GWB amplitudes in **coarse** pixels

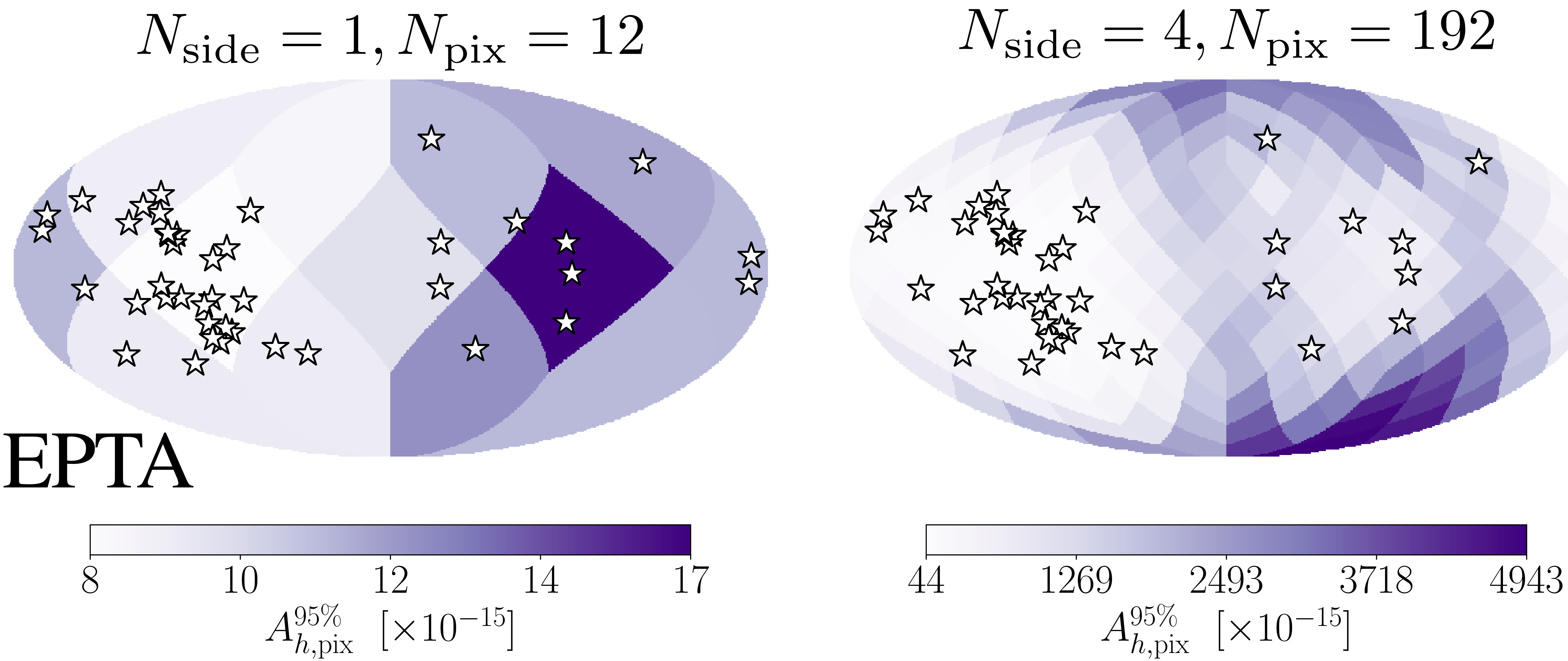

Sensitivity to the monopole (i.e. average GWB amplitude):

- 1 single pixel (i.e. pure monopole): $A_h^{95\%} = 2.5 \times 10^{-15}$
- 12 pixels: $A_h^{95\%} = 5.0 \times 10^{-15}$
- 192 pixels: $A_h^{95\%} = 7.8 \times 10^{-15}$

Example 2: spherical harmonic amplitudes

$$\mathcal{A}(\hat{\Omega}) = \sum_{\ell,m} \mathcal{A}_{\ell m} Y_{\ell m}(\hat{\Omega}) \qquad \mathcal{C}_\ell \equiv \frac{1}{2\ell+1} \sum_m |\mathcal{A}_{\ell m}|^2$$

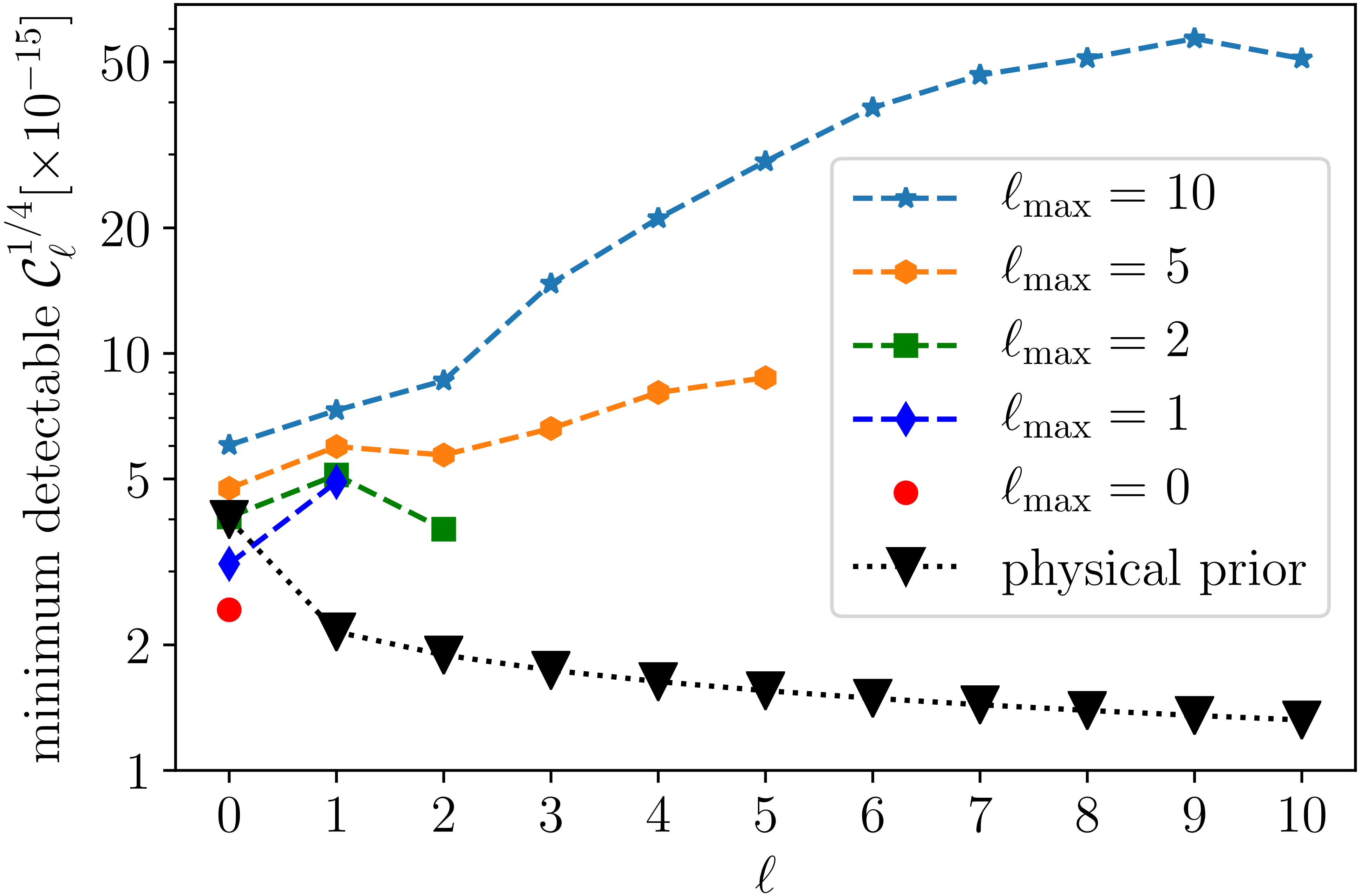

Searching for anisotropies of known shape

Issue: sensitivity to each coefficient (including monopole), systematically degrades when including more basis maps.

In other words, with standard basis maps, forecasts are dependent on assumed cutoff.

Reason: standard basis maps are statistically correlated.

➡ One needs to have **robust priors** on the basis maps present in the data to make meaningful forecasts.

Agnostic searches for anisotropies

Taylor et al 2015: derive $N_{\rm pix} = 12288$ "upper limit map"
using 6 EPTA pulsars, i.e. 15 pairs

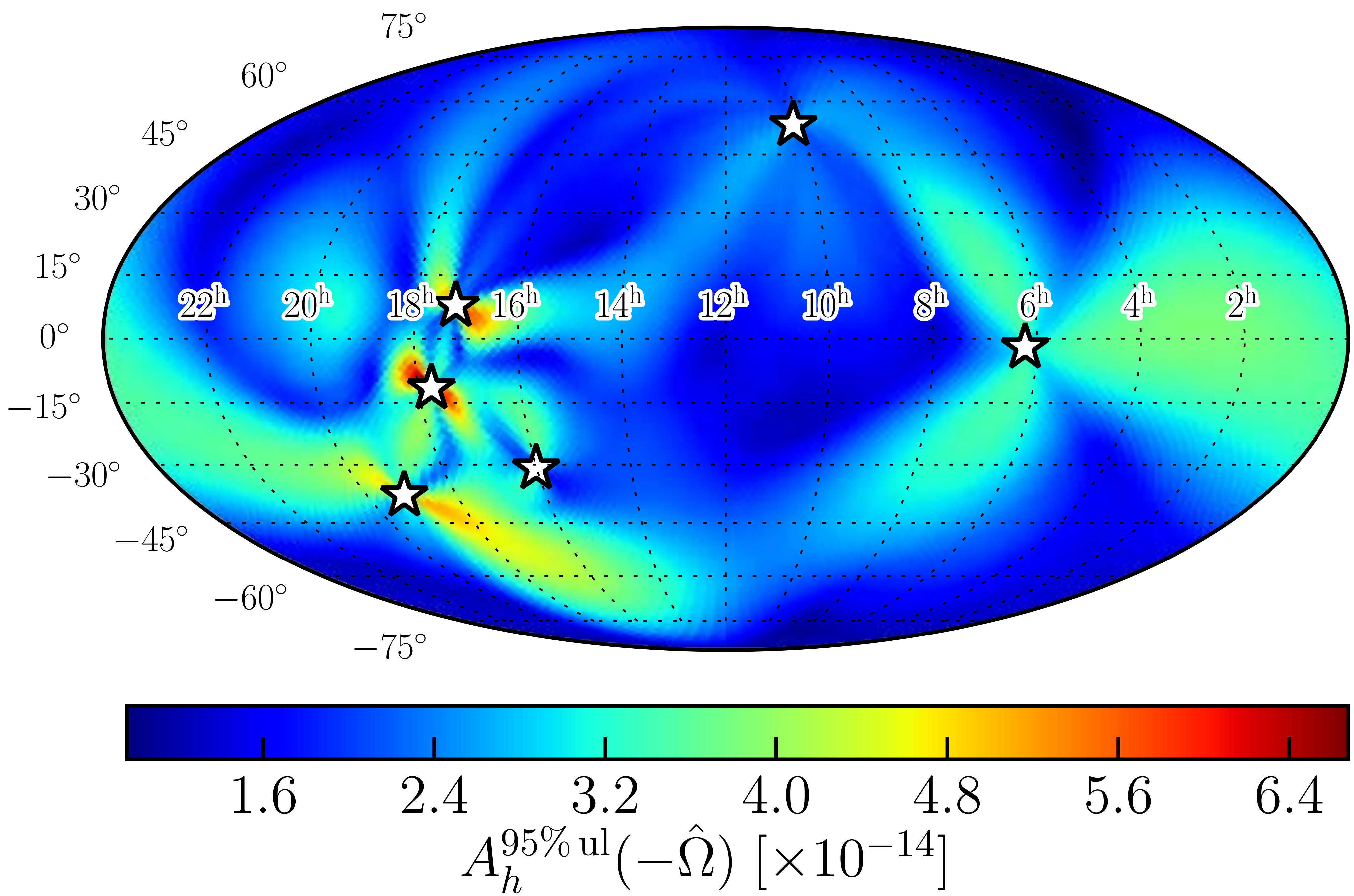

This map represent constraints on the observable component only

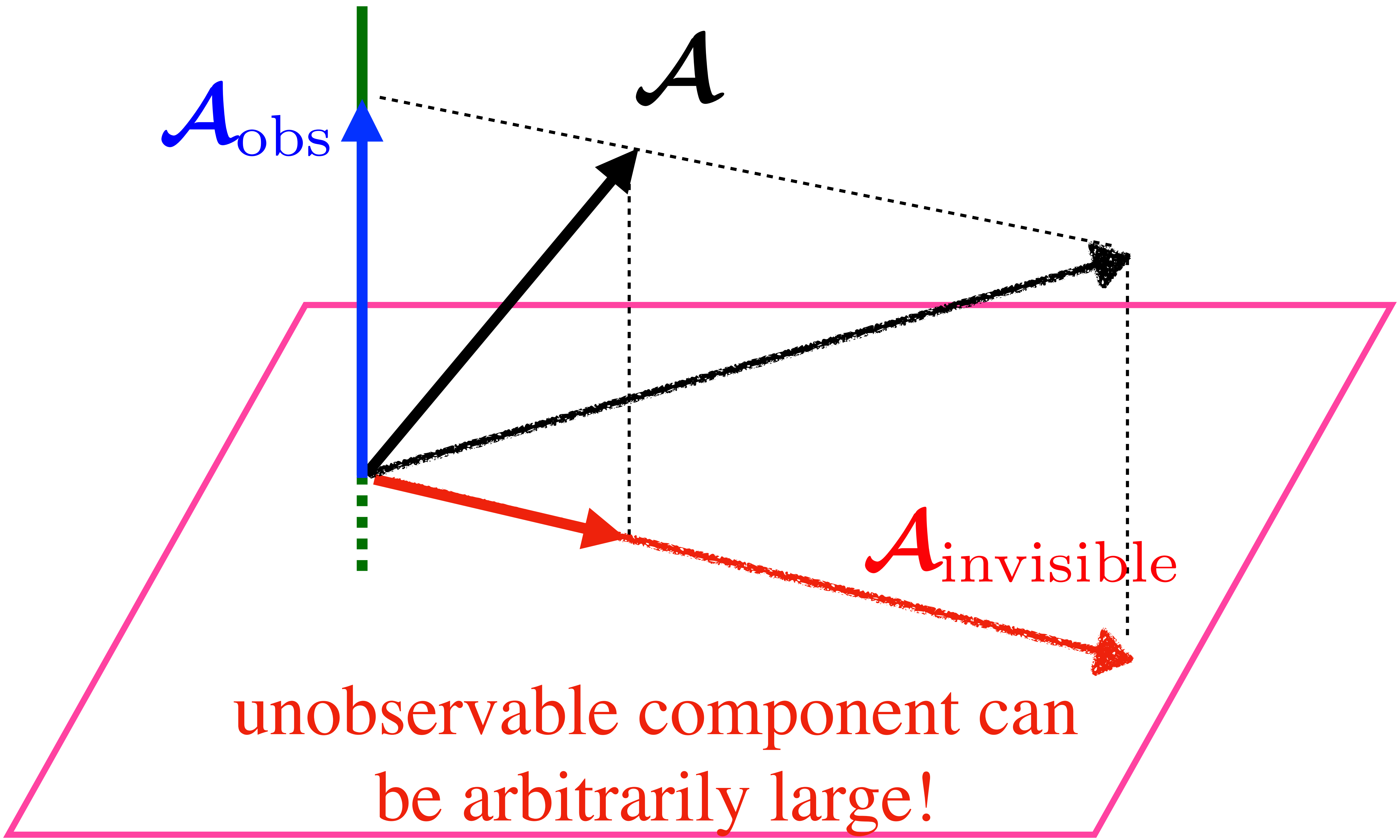

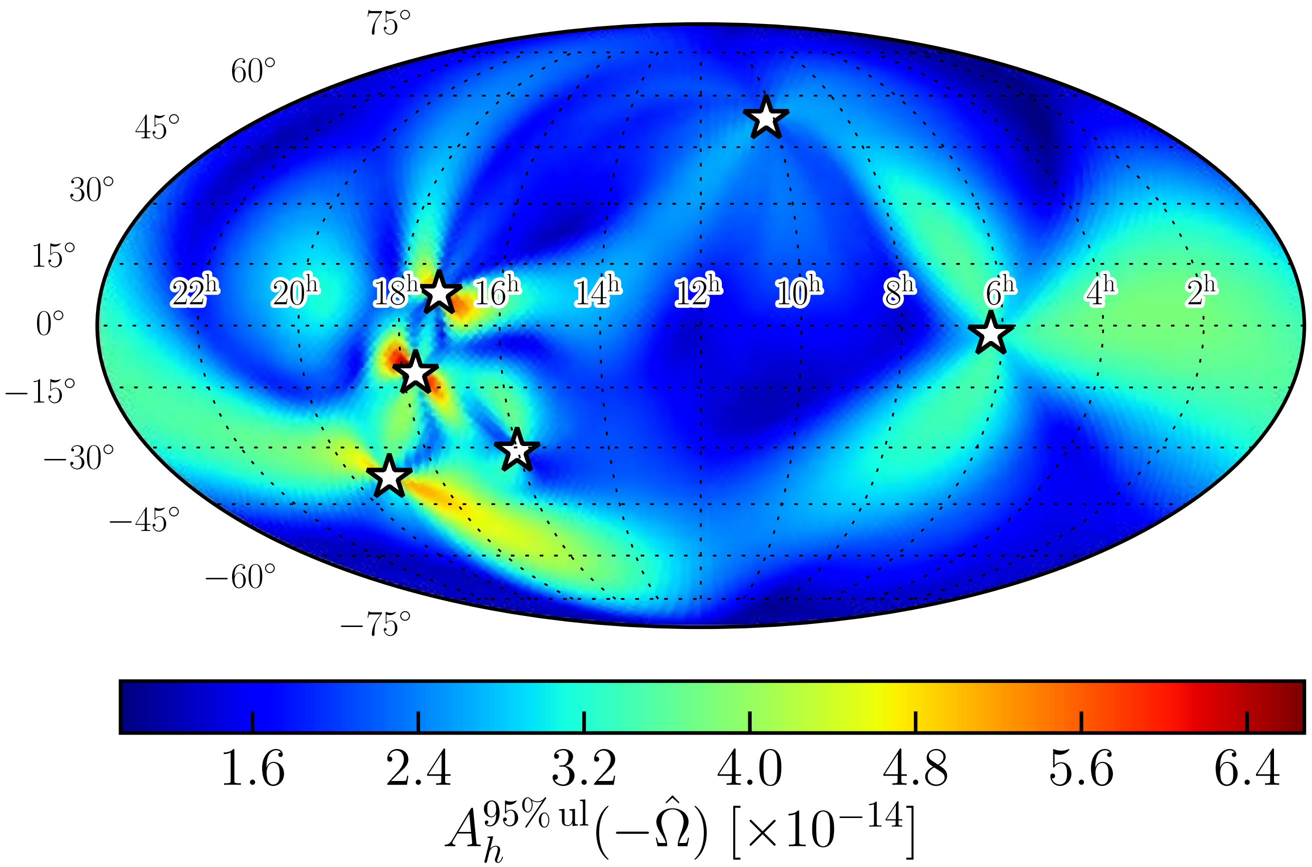

Taylor et al. 2015

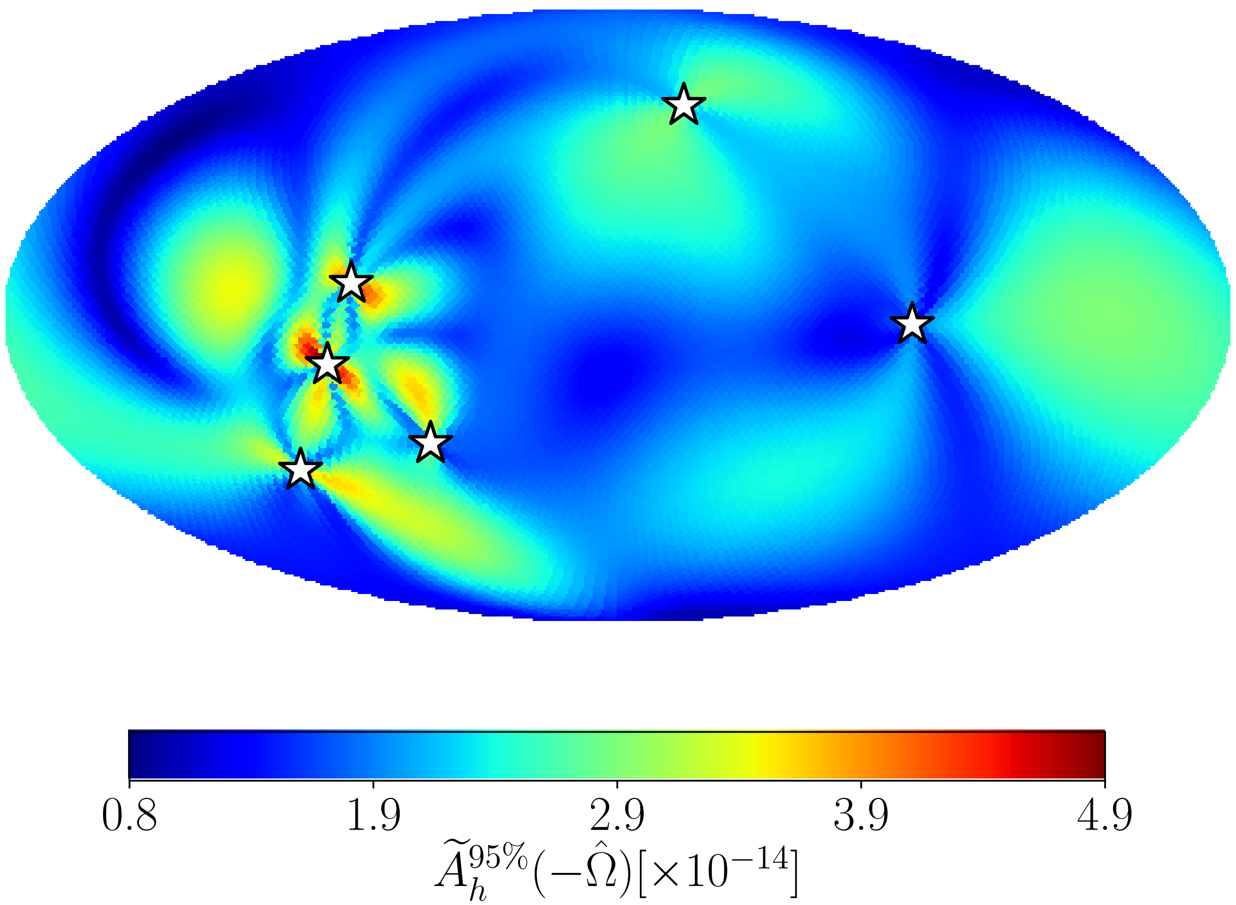

Our ``forecast" for this map

These are **not upper limits** on the GWB in each pixel

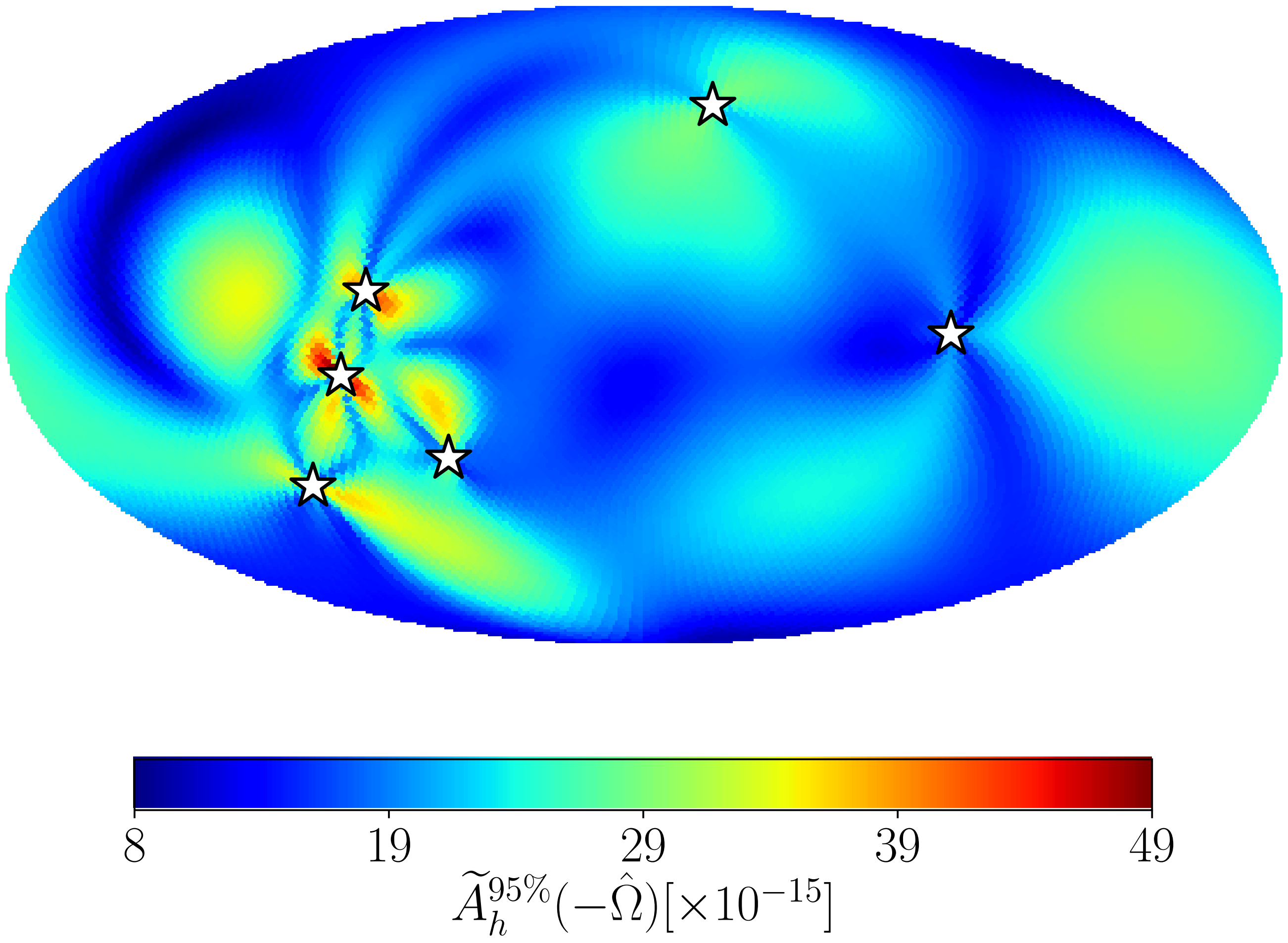

Our ``forecast” for this map

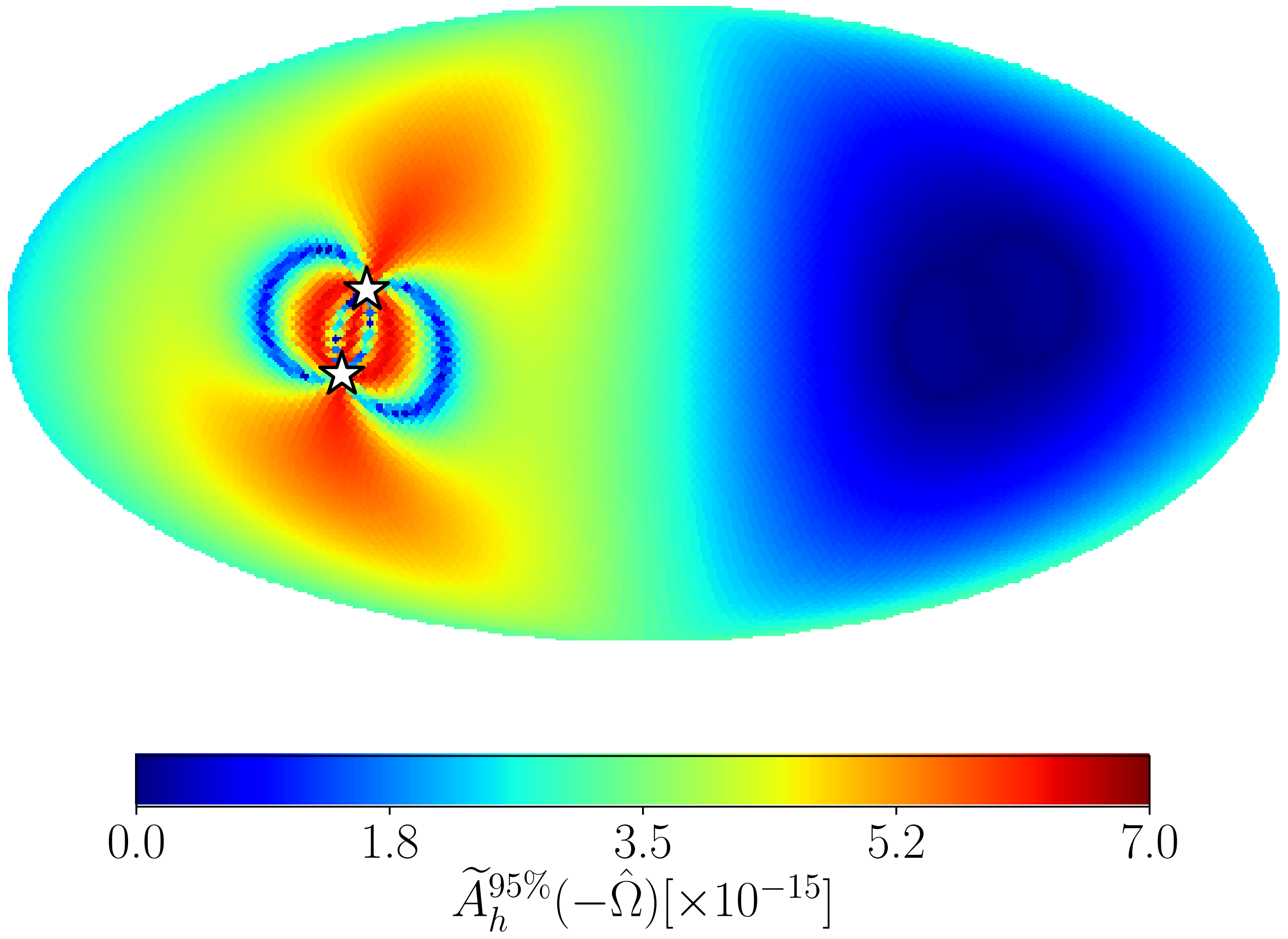

Equivalent map with 1 pair only. The observable space is smaller (1-dimensional), better “constraints”

These are **not upper limits** on the GWB in each pixel

Agnostic searches for anisotropies

"Principal maps" = eigenmaps of the Fisher matrix

➡ $N_{\rm pair}$ statistically independent GWB maps spanning the space of observable maps

➡ Can search of the amplitudes of all principal maps simultaneously without increasing the noise of each one.

➡ Allow to search under the PTA lampost

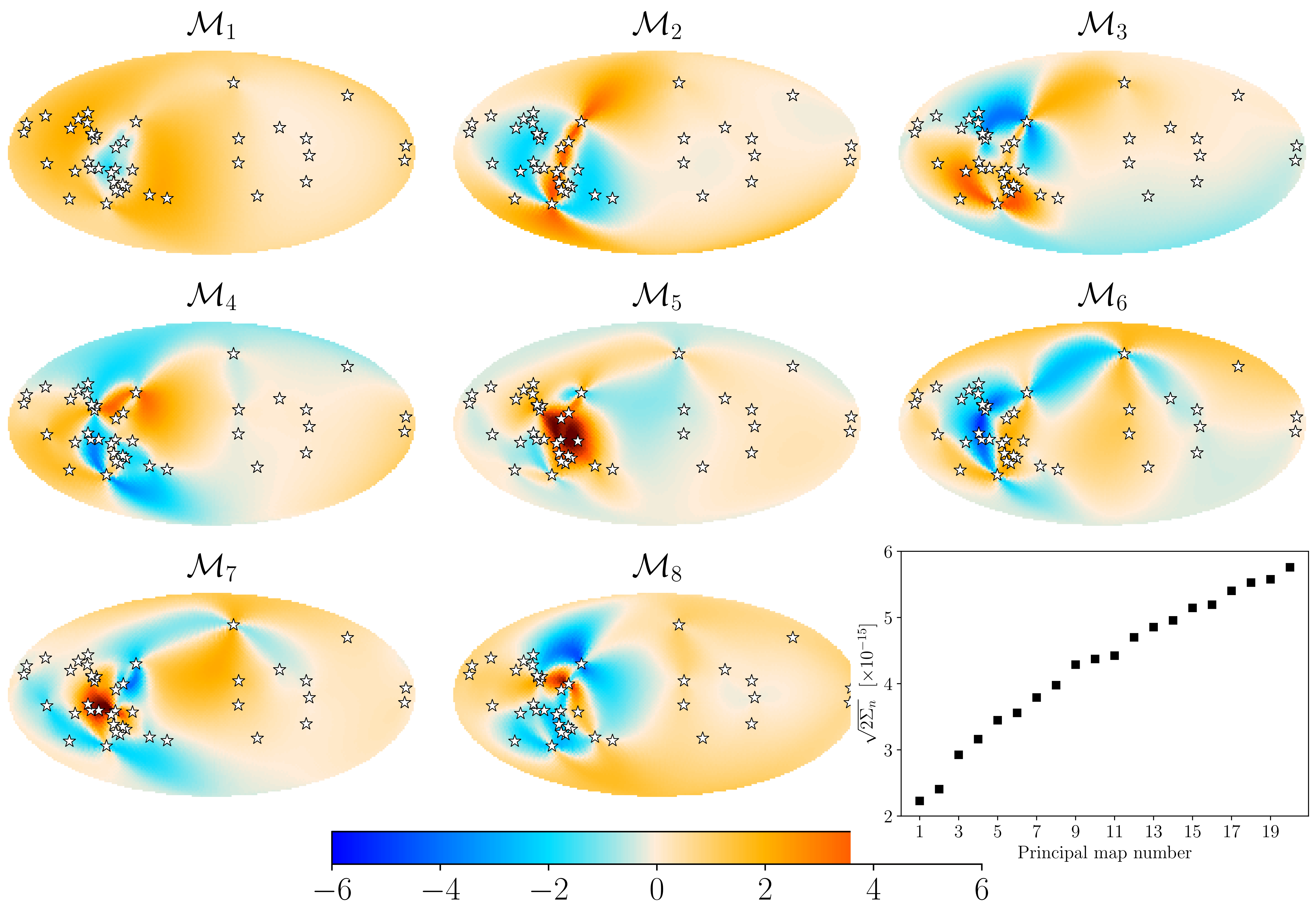

Issue: have to give up the monopole as a “preferred map”

“Reconstructing” the (observable part of the) GWB

- Search for amplitudes $\widehat{A}_n$ of all principal maps

- Define the reconstructed map as

$$\boldsymbol{\mathcal{A}}_{\rm recon} \equiv \sum_{n;{\rm SNR}_n>3} \widehat{A}_n\, \boldsymbol{\mathcal{M}}_n$$

- Similar to making a “dirty map” in radio interferometry: keep only the measured pieces of information and set the non-measured ones to zero.

- Note: the reconstructed map still formally has “infinite error bars” due to unobservable component…

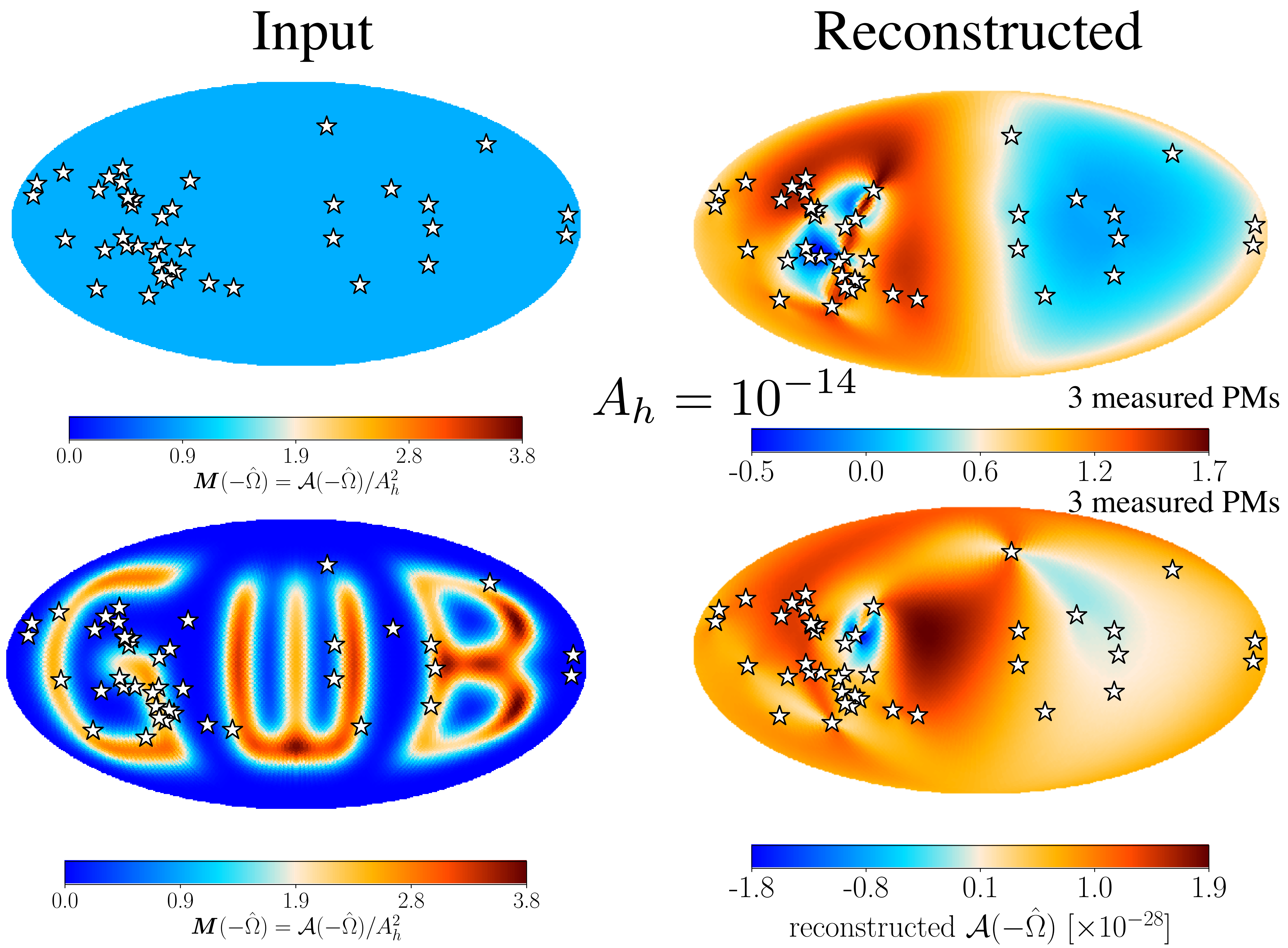

Input
Reconstructed
$A_h = 10^{-14}$
3 measured PMs
0.0 0.9 1.9 2.8 3.8
$\boldsymbol{M}(-\hat{\Omega}) = \mathcal{A}(-\hat{\Omega})/A_h^2$
-0.5 0.0 0.6 1.2 1.7
3 measured PMs
0.0 0.9 1.9 2.8 3.8
$\boldsymbol{M}(-\hat{\Omega}) = \mathcal{A}(-\hat{\Omega})/A_h^2$
-1.8 -0.8 0.1 1.0 1.9
reconstructed $\mathcal{A}(-\hat{\Omega})$ $[\times 10^{-28}]$

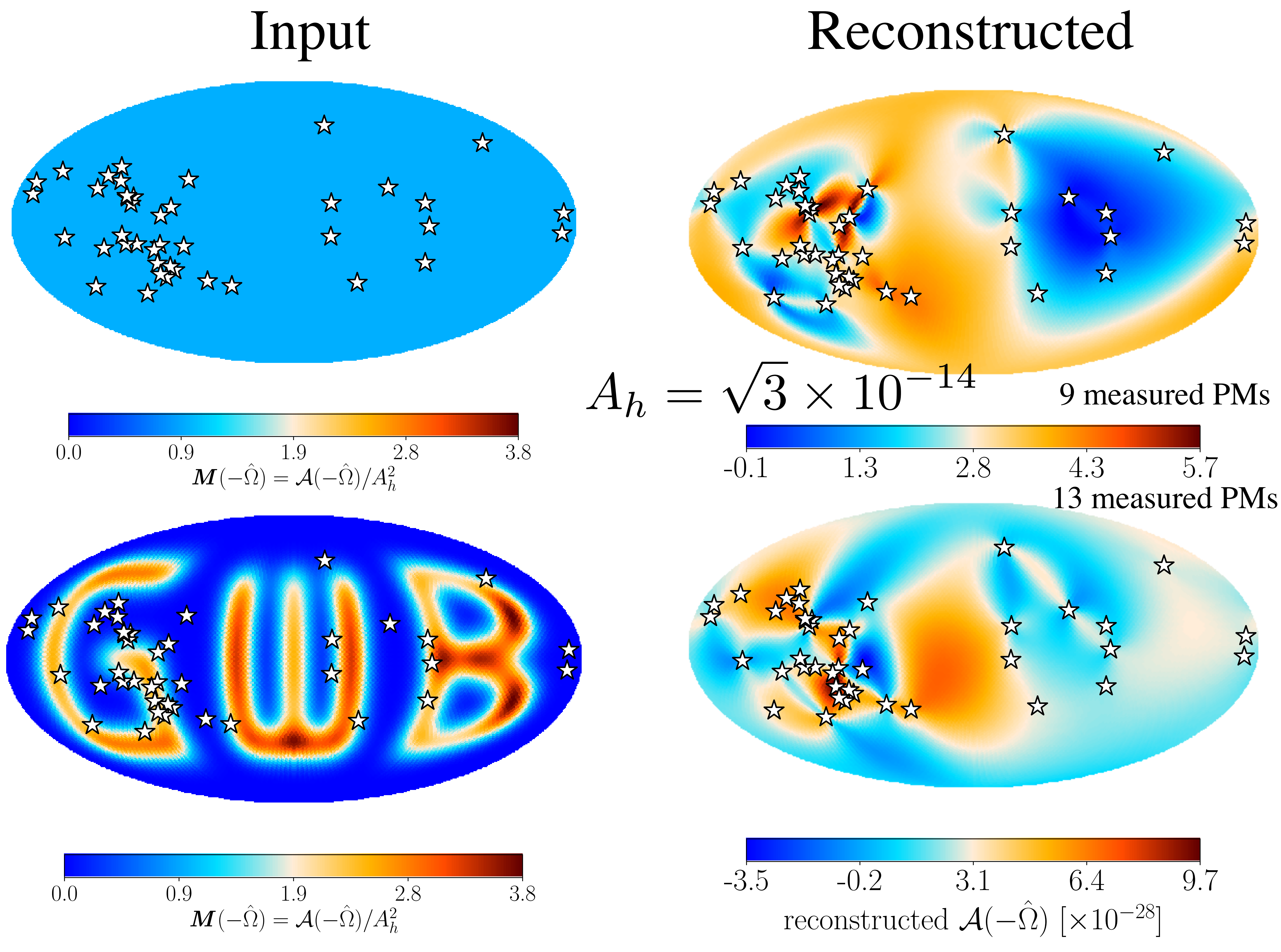

Input
Reconstructed
$A_h = \sqrt{3} \times 10^{-14}$
9 measured PMs
0.0 0.9 1.9 2.8 3.8
$\boldsymbol{M}(-\hat{\Omega}) = \mathcal{A}(-\hat{\Omega})/A_h^2$
-0.1 1.3 2.8 4.3 5.7
13 measured PMs
0.0 0.9 1.9 2.8 3.8
$\boldsymbol{M}(-\hat{\Omega}) = \mathcal{A}(-\hat{\Omega})/A_h^2$
-3.5 -0.2 3.1 6.4 9.7
reconstructed $\mathcal{A}(-\hat{\Omega})$ $[\times 10^{-28}]$

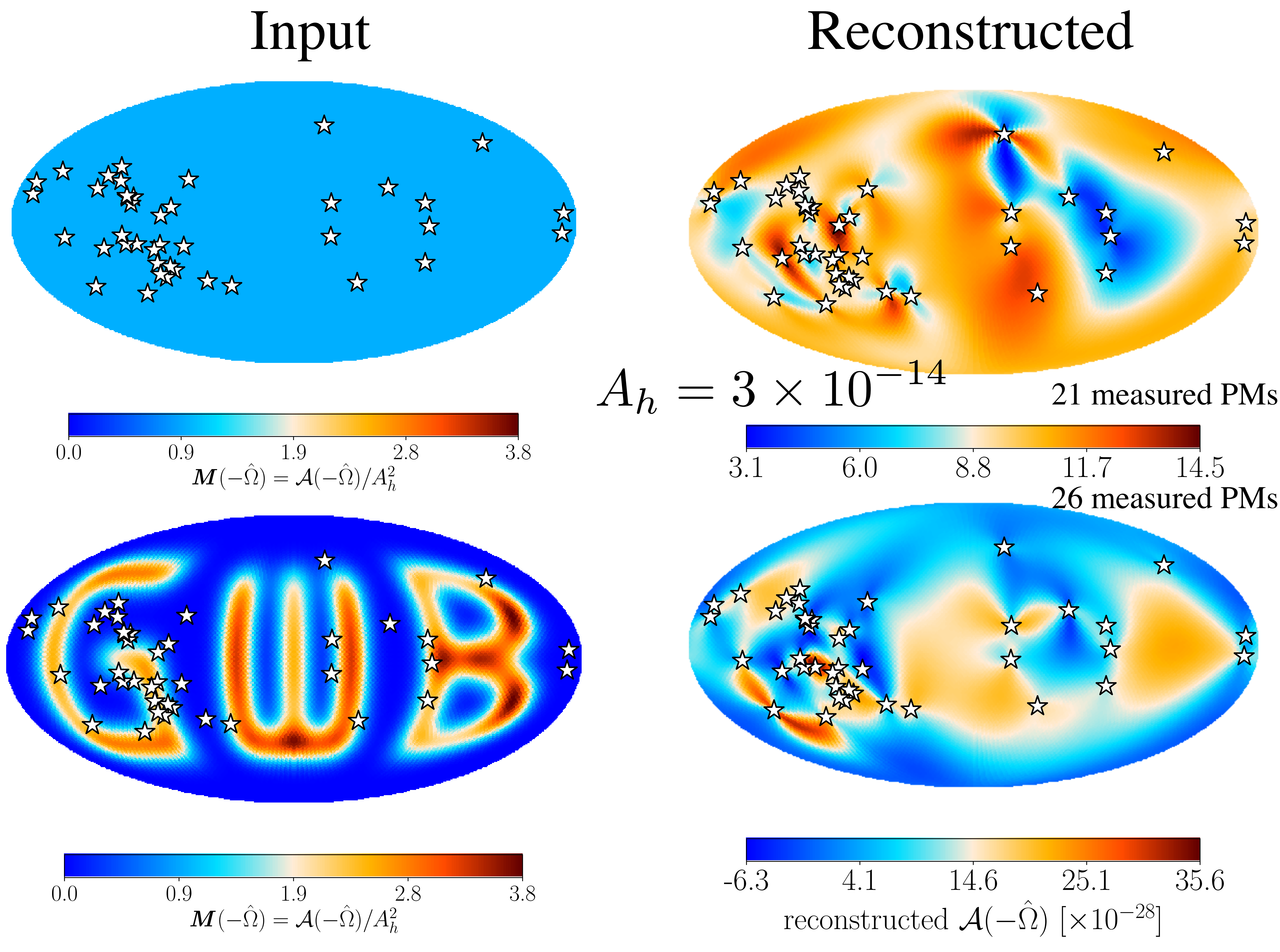

Input
Reconstructed
$A_h = 3 \times 10^{-14}$
21 measured PMs
26 measured PMs
0.0
0.9
1.9
2.8
3.8
$\boldsymbol{M}(-\hat{\Omega}) = \mathcal{A}(-\hat{\Omega})/A_h^2$
3.1
6.0
8.8
11.7
14.5
-6.3
4.1
14.6
25.1
35.6
reconstructed $\mathcal{A}(-\hat{\Omega})$ $[\times 10^{-28}]$

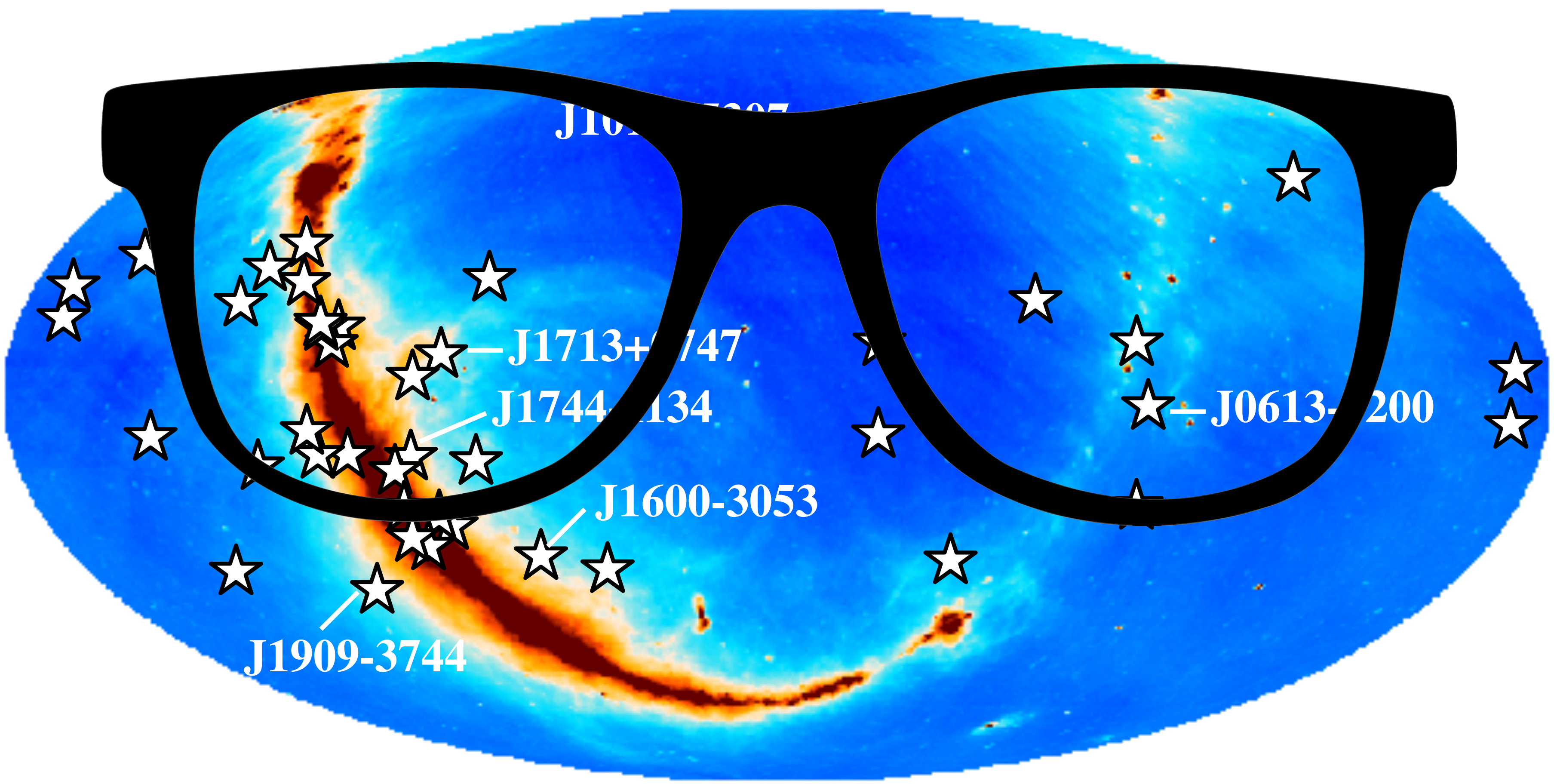

Alternative approach: examine the best-fit chi-squared, and ask whether it is consistent with pure monopole. Allows to assess presence of anisotropies in data, but not their specific shape (see paper).

Conclusions — anisotropies

- N_{pair} independent components is all you get, at most!
- Searching for monopole + standard anisotropies systematically degrades the sensitivity to all amplitudes
- One can search for GWB anisotropies "under the lamppost" with principal maps. Requires a large signal with current PTAs.

➡ Prospects for detecting unknown GWB anisotropies with current PTAs appear limited

- **Future work: search for statistical anisotropies**

Future extensions

- Include more realistic sources of correlated noise

— **Global clock errors:** fully correlated between different pulsars, independent of angle between pulsars:

$$\langle R_p^{\rm clock}(f) R_q^{*\rm clock}(f)\rangle = \mathcal{P}^{\rm clock}(f)$$

— **Ephemerides errors** $R_p^{\rm eph}(f) = \hat{p}\cdot\vec{V}(f)$

$$\langle R_p^{\rm eph}(f) R_q^{*\rm eph}(f)\rangle = \hat{p}^i\hat{p}^j\mathcal{P}_{ij}^{\rm eph}(f)$$

- Beyond the weak-signal limit (weak anisotropy limit)?

- In general, build a robust and efficient forecasting tool